ORIGINAL PAPER

Marcela A. Cruchaga · Diego J. Celentano
Tayfun E. Tezduyar

Collapse of a liquid column: numerical simulation and experimental validation

Abstract This paper is focused on the numerical and experimental analyses of the collapse of a liquid column. The measurements of the interface position in a set of experiments carried out with shampoo and water for two different initial column aspect ratios are presented together with the corresponding numerical predictions. The experimental procedure was found to provide acceptable recurrence in the observation of the interface evolution. Basic models describing some of the relevant physical aspects, e.g. wall friction and turbulence, are included in the simulations. Numerical experiments are conducted to evaluate the influence of the parameters involved in the modeling by comparing the results with the data from the measurements. The numerical predictions reasonably describe the physical trends.

Keywords Moving interfaces · Two-fluid flows · Computational fluid mechanics · Experimental validation

1 Introduction

Modeling two-liquid interfaces or free-surface flows is an active research field due to the wide range of their engineering applications. This motivates the development of formulations capable of accurately representing this kind of transient problems. Various numerical techniques were proposed, with moving or fixed domain discretizations, to overcome the challenges related to updating the interface intrinsically coupled with the fluid dynamics equations (e.g. see [1–34], and references therein). Work was carried out also in the development of physical models to represent real problems at laboratory scales and, in particular, to assess the numerical performance

M.A. Cruchaga (✉) · D.J. Celentano
Departamento de Ingeniería Mecánica,
Universidad de Santiago de Chile,
Av. Bdo. O'Higgins 3363, Santiago, Chile
E-mail: mcruchag@lauca.usach.cl

T.E. Tezduyar
Team for Advanced Flow Simulation and Modeling (T*AFSM),
Mechanical Engineering, Rice University - MS 321,
Houston, TX 77005, USA

of the proposed numerical techniques by comparing their predictions with the measurements obtained from experiments. Focusing on the description of the collapse of a water column, experiments were presented in [11, 35]. This problem was adopted by several researchers as a benchmark test to validate the numerical performance of the proposed formulations in solving two-liquid interfaces or free-surface flows [11, 12, 15, 21, 23, 24, 26, 28, 29, 32].

In this paper, in addition to numerical results, we report results from experiments for the collapse of liquid columns. The experiments are carried out using two different fluids: shampoo and water, and two different column aspect ratios (height to width ratio of the initial liquid column). The purpose of these experiments is to provide data for the interface evolution with very different fluid properties. The experimental data is used for evaluating the performance of the numerical formulations we propose for solving this class of problems.

We use finite element techniques with fixed meshes. The interface is "captured" by solving an advection equation governing the time-evolution of an interface function that marks the interface location [16–33]. A version of this approach presented in [32] can capture the interface while maintaining the global mass conservation and accurately representing the sudden changes in the materials properties. That formulation is called the edge-tracked interface locator technique (ETILT), which was introduced in [19]. More recent versions of the ETILT were introduced in [30, 31, 33]. Although some new techniques related to the ETILT are presented in this work, the simulations are mainly devoted to evaluation of the numerical performance of our core techniques in describing some of the physical aspects such as wall friction and turbulence. The influence of the parameters involved in modeling is also analyzed.

The governing equations are presented in Sect. 2. The ETILT and the new aspects included in its current version are summarized in Sect. 3. The details of the experimental procedure are presented in Sect. 4. Experimental and numerical results are presented and discussed in Sect. 5. Concluding remarks are presented in Sect. 6.
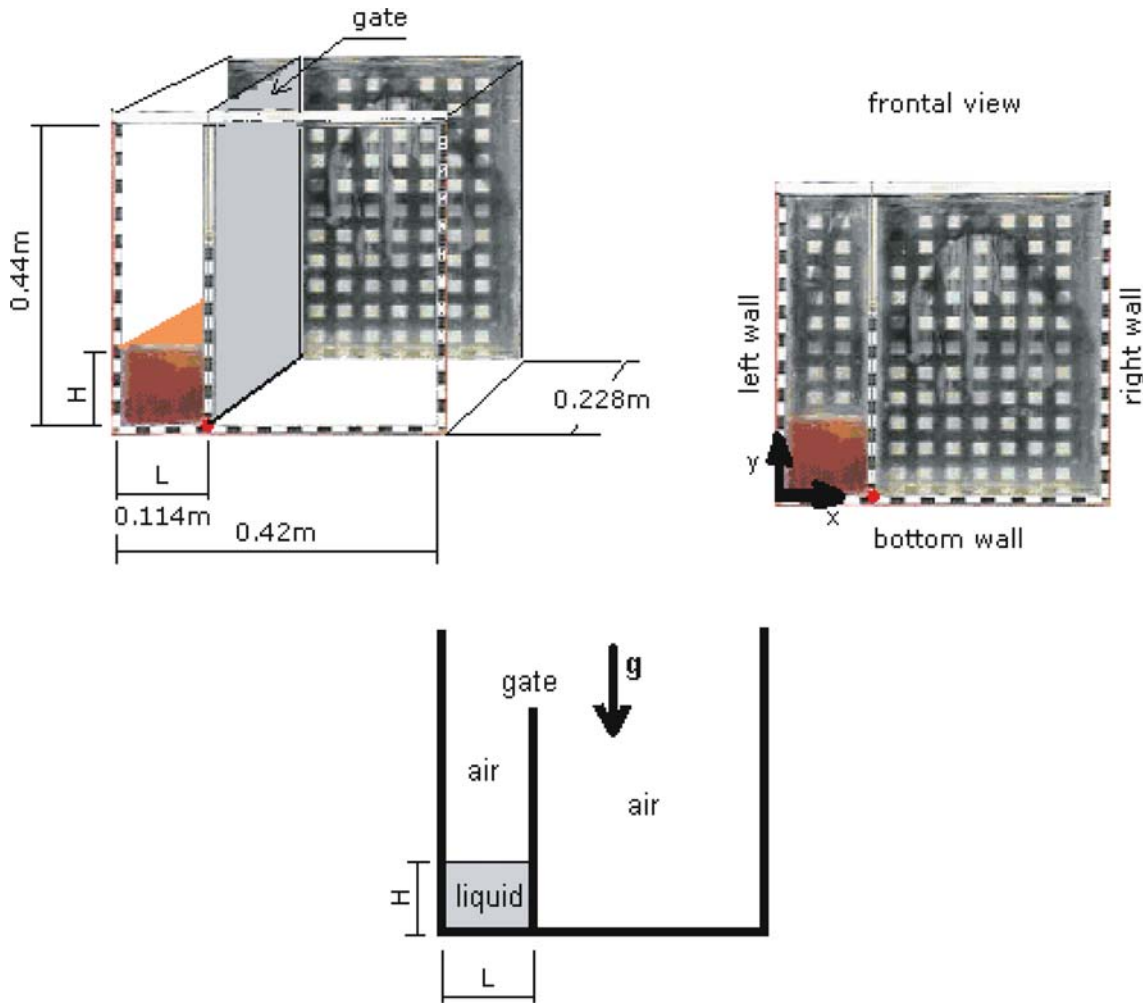
Fig. 1 Collapse of a liquid column: experimental setup and illustrative picture

2 Governing equations

The Navier–Stokes equations of unsteady incompressible flows are written as follow:

$$\rho \frac{\partial \mathbf{u}}{\partial t} + \rho \mathbf{u} \nabla \cdot \mathbf{u} + \nabla p - \nabla \cdot (2\mu \varepsilon) = \rho \mathbf{f} \quad \text{in } \Omega \times Y, \quad (1)$$

$$\nabla \cdot \mathbf{u} = 0 \quad \text{in } \Omega \times Y, \quad (2)$$

where ρ, $\mathbf{u}$, p, μ, ε and $\mathbf{f}$ are the density, velocity, pressure, dynamic viscosity, strain-rate tensor, and the specific body force. In these equations, Ω denotes an open-bounded domain with a smooth boundary Γ, and Y is the time interval of interest. This system of equations is completed with a set of initial and boundary conditions:

$$\mathbf{u} = \mathbf{u}_0 \quad \text{in } \Omega \quad (3)$$

$$\mathbf{u} = \mathbf{g} \quad \text{in } \Gamma_g \times Y \quad (4)$$

$$\sigma \cdot \mathbf{n} = \mathbf{h} \quad \text{in } \Gamma_h \times Y \quad (5)$$

where $\mathbf{u}_0$ is the initial value of the velocity field, $\mathbf{g}$ represents the velocity imposed on the part of the boundary Γ_g, and $\mathbf{h}$ is the traction vector imposed over Γ_h ($\Gamma_g \cup \Gamma_h = \Gamma$ and $\Gamma_g \cap \Gamma_h = \emptyset$), typically taken as traction-free condition: $\mathbf{h} = \mathbf{0}$.

In the present simulations, the condition at a friction wall is given by the following simple model [21]:

$$\mathbf{h} = -\frac{\rho \mathbf{u} |\mathbf{u}|}{C_f^2} \quad \text{in } (\Gamma_h)_w \times Y, \quad (6)$$

where C_f is a friction parameter and $(\Gamma_h)_w$ is a subset of Γ_h, representing the walls where the friction conditions are applicable.

A simple model to compute the energy dissipated by the turbulent effects could be obtained by modifying μ as [32]:

$$\mu = \min(\mu + l_{\text{mix}}^2 \rho \sqrt{2\varepsilon : \varepsilon}; \mu_{\text{max}}), \quad (7)$$

where l_{mix} is a characteristic mixing length (in the present work, $l_{\text{mix}} = C_t h_{\text{UGN}}$ with C_t being a modeling parameter and h_{UGN} a characteristic element length [20]) and μ_{max} is a cut-off value.
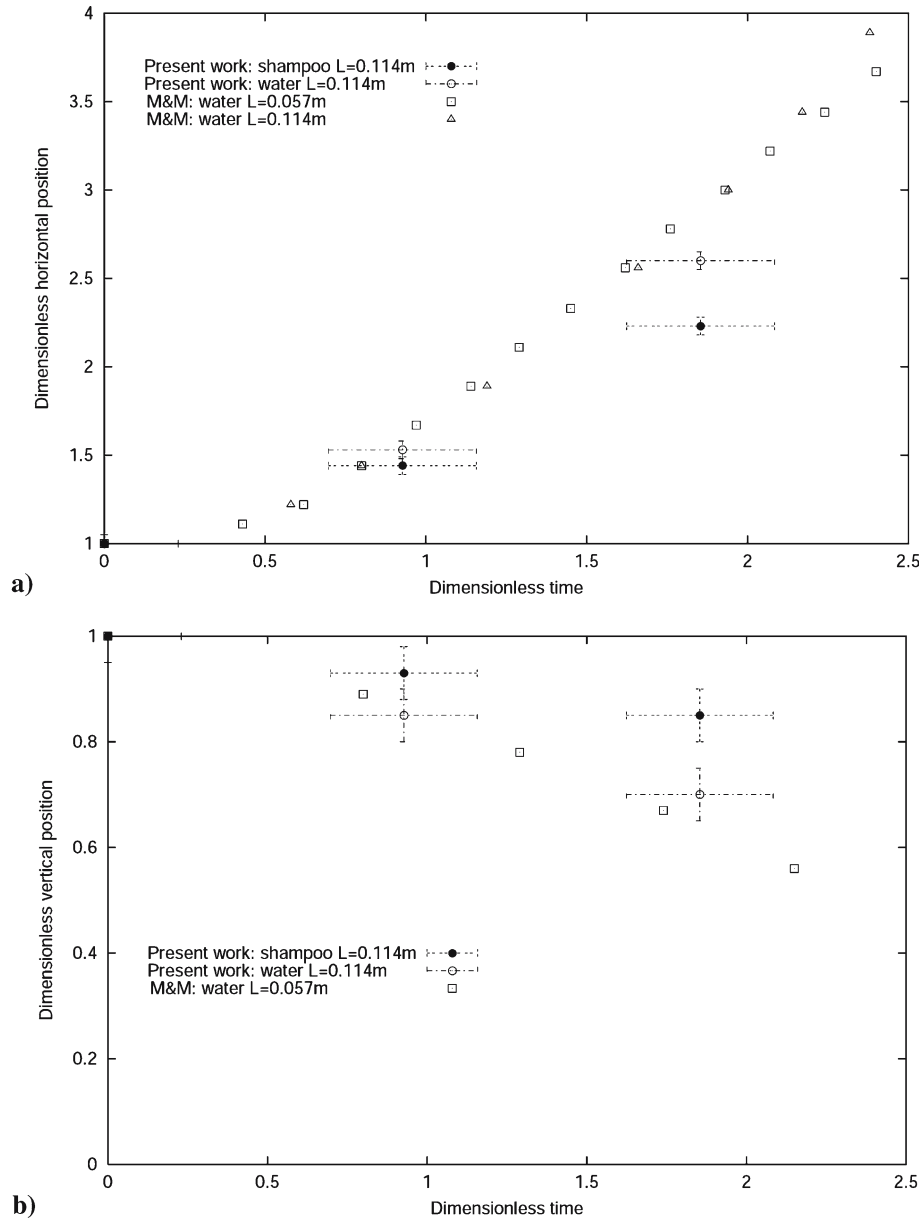
Fig. 2 Collapse of a liquid column for aspect ratio $A_r = 1$. Experimental results for the time evolution of the interface position: **a** dimensionless horizontal position (x/L) at $y = 0.0$ m (*bottom wall*) and **b** dimensionless vertical position (y/L) at $x = 0.0$ m (*left wall*). Comparison with the results obtained by Martin and Moyce (M&M) [35]

The interface between the two fluids (Fluids 1 and 2) represents a strong discontinuity in the fluid properties and the gradients of the velocity and pressure. Nevertheless, these variables are interpolated as continuous functions across the interface. Other types of discontinuities at the interface, e.g. surface tension, are not included in the present model. The interface motion is governed by an advection equation:

$$\frac{\partial \varphi}{\partial t} + \mathbf{u} \cdot \nabla \varphi = 0 \quad \text{in } \Omega \times Y, \tag{8}$$

where φ is a function marking the location of the interface.

The weak form of the Navier–Stokes equations is obtained in the context of a finite element formulation using a Generalized Streamline Operator technique [34]. The stabilized nature of the technique allows the use of equal-order interpolation functions for velocity and pressure. In the context of two-fluid flow analysis, all the matrices and vectors derived from the discrete form are computed including the discontinuity in fluid properties [32]. Therefore, the algorithm used for updating the interface is coupled with the finite element solution of the Navier–Stokes equations. The time integration is performed using a standard backward Euler scheme.
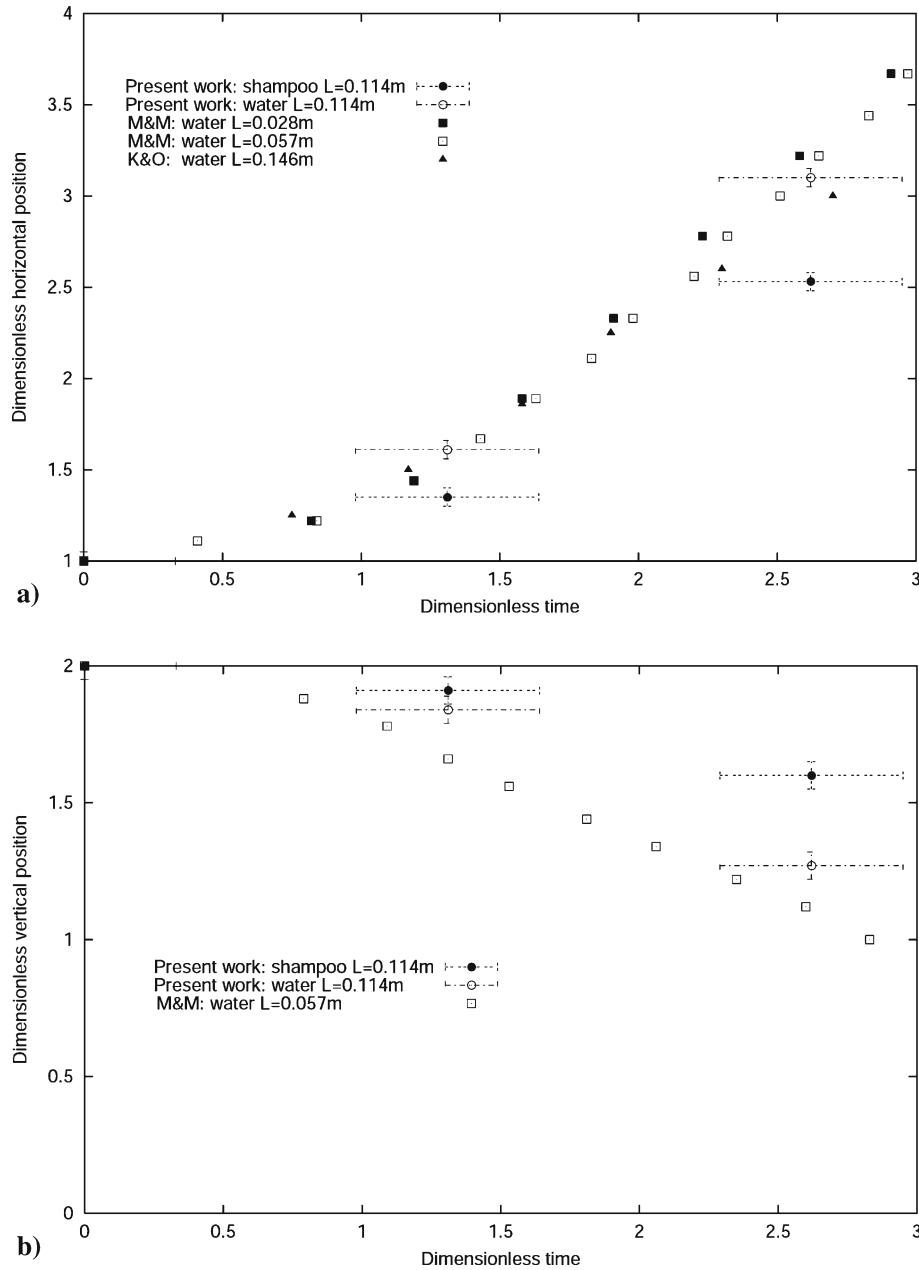
Fig. 3 Collapse of a liquid column for aspect ratio $A_r = 2$. Experimental results for the time evolution of the interface position: **a** dimensionless horizontal position (x/L) at $y = 0.0$ m (*bottom wall*) and **b** dimensionless vertical position (y/L) at $x = 0.0$ m (*left wall*). Comparison with the results obtained by Martin and Moyce (M&M) [35] and Koshizuka and Oka (K&O) [11]

3 Interface update

In the present work, the version of the ETILT presented in [32] is used for updating the interface. At each time step, Eqs. (1) and (2) are computed in the entire domain using the density and viscosity distributions expressed as:

$$\rho^h = \varphi^{he}\rho_1 + (1 - \varphi^{he})\rho_2, \qquad (9.1)$$

$$\mu^h = \varphi^{he}\mu_1 + (1 - \varphi^{he})\mu_2, \qquad (9.2)$$

where φ^{he} is the edge-based representation of φ.

To determine $\mathbf{u}^h_{n+1}$, p^h_{n+1} and φ^{he}_{n+1} at a time level $n + 1$ from $\mathbf{u}^h_n$ and φ^{he}_n at time level n, the velocity and pressure are computed from Eqs. (1) and (2). To compute φ^{he}_{n+1}, given φ^{he}_n, first a nodal representation φ^h is computed. This is done by using a constrained least-squares projection as given in [30, 33]:
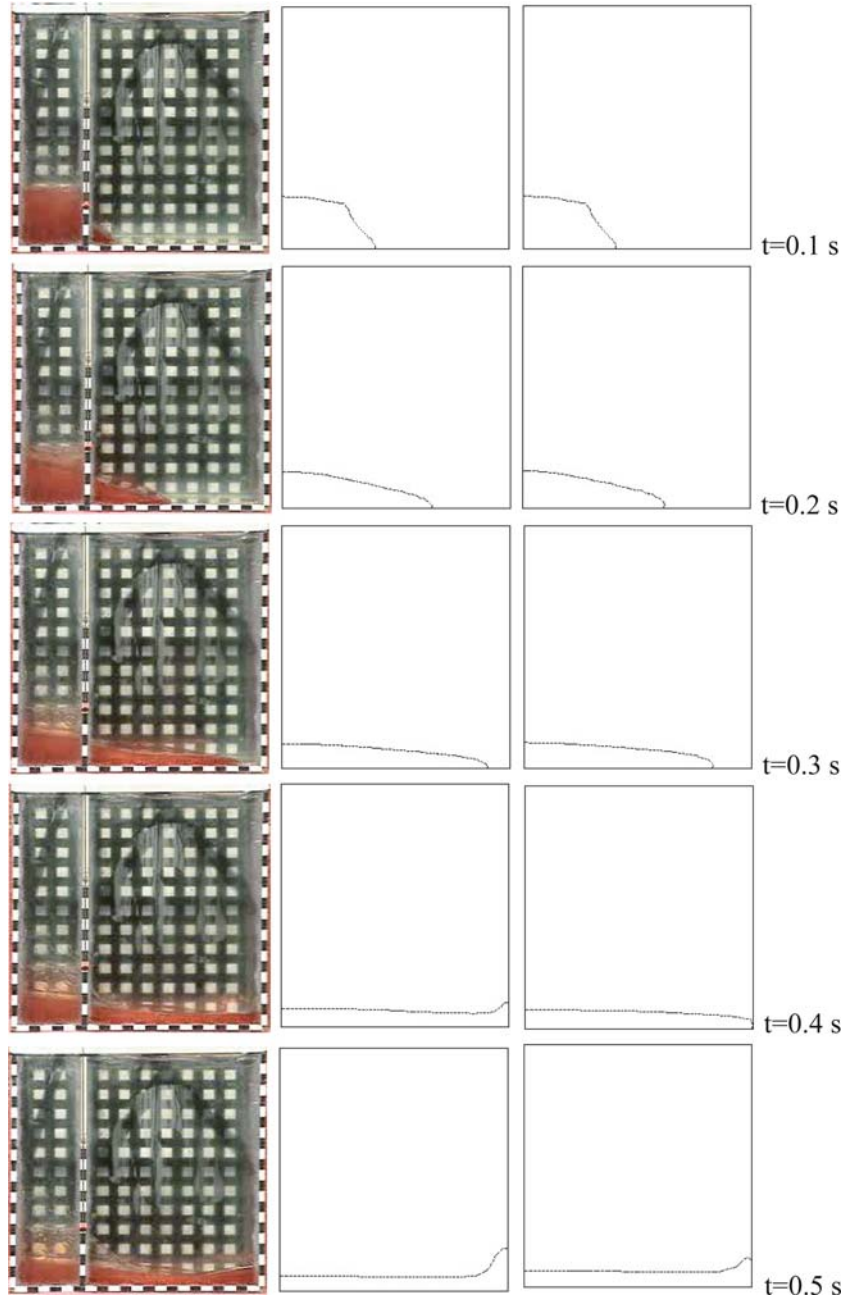
Fig. 4 Collapse of a shampoo column with aspect ratio $A_r = 1$. Interface positions at different instants: experimental (*left*) and numerical results computed without (Simulation 1, *middle*) and with (Simulation 2, *right*) wall friction effects

$$\int_\Omega \psi^h \left(\varphi_n^h - \varphi_n^{he} \right) d\Omega$$

$$+ \sum_{k=1}^{n_{ie}} \psi^h(\mathbf{x}_k) \lambda_{PEN} \left(\varphi_n^h(\mathbf{x}_k) - 0.5 \right) = 0. \tag{10}$$

Here ψ^h is the test function, n_{ie} is the number of the interface edges (i.e., the edges crossed by the interface), $\mathbf{x}_k$ is the coordinate of the interface location along the kth interface edge and λ_{PEN} is a penalty parameter. This penalty parameter ensures that the projection topologically preserves the interface position along edges. In four-noded quadrilateral elements, this condition is activated also along the element diagonals crossed by the interface. After this projection, we update the interface by using a discretization based on the streamline upwind/Petrov–Galerkin (SUPG) formulation [1] of the advection equation (8) governing φ:
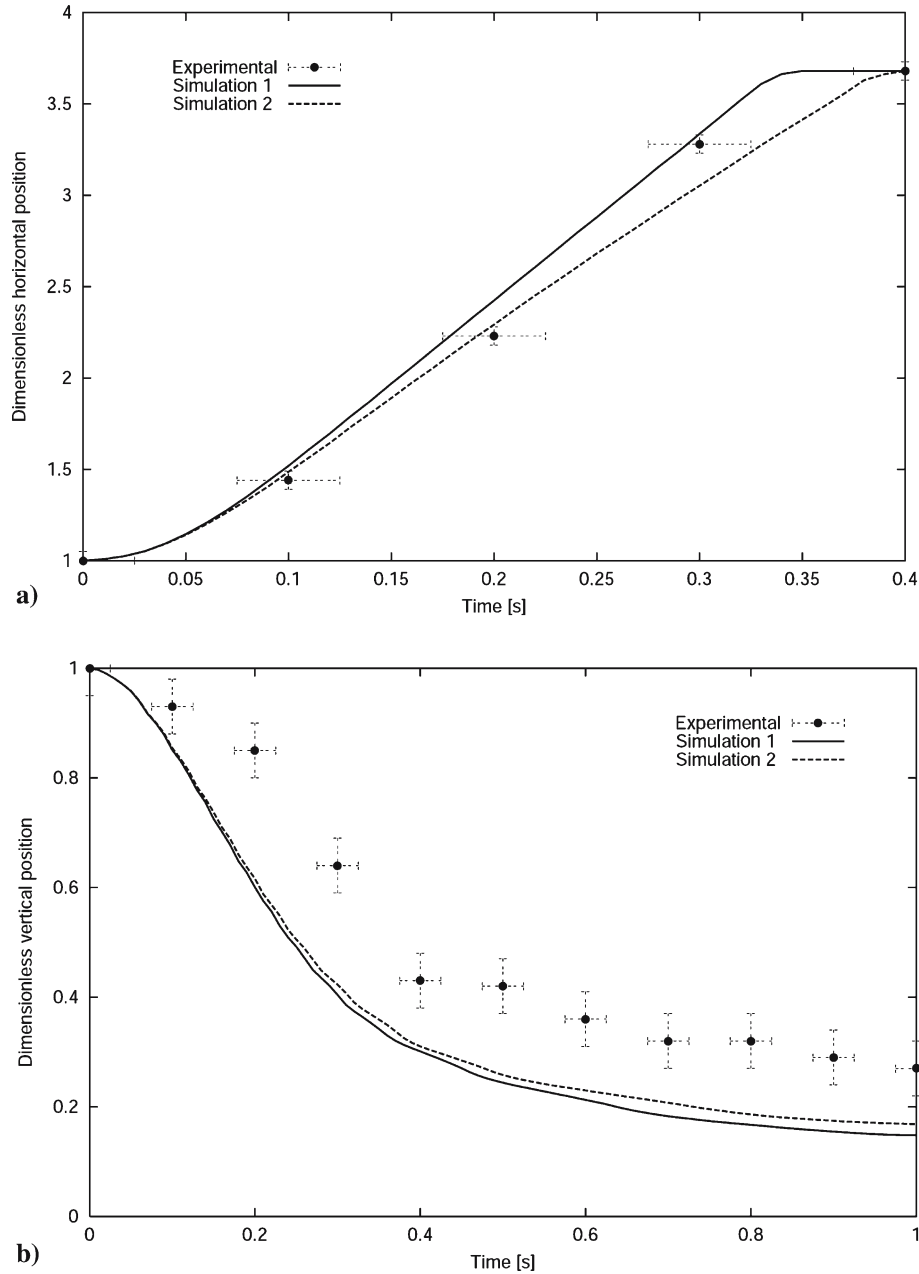
Fig. 5 Collapse of a shampoo column with aspect ratio $A_r = 1$: **a** dimensionless horizontal position (x/L) at $y = 0.0$ m (*bottom wall*), **b** dimensionless vertical position (y/L) at $x = 0.0$ m (*left wall*), **c** dimensionless vertical position (y/L) at $x = 0.27$ m (*middle of the box*) and **d** dimensionless vertical position (y/L) $x = 0.42$ m (*right wall*). Numerical results computed without (Simulation 1) and with (Simulation 2) wall friction effects

$$\int_\Omega \psi^h \left(\frac{\partial \varphi^h}{\partial t} + \mathbf{u}^h . \nabla \varphi^h \right) d\Omega$$

$$+ \sum_{e=1}^{n_{el}} \int_{\Omega^e} \left(\tau_{\mathrm{SUPG}} \mathbf{u}^h . \nabla \psi^h \right) \left(\frac{\partial \varphi^h}{\partial t} + \mathbf{u}^h . \nabla \varphi^h \right) d\Omega$$

$$+ \sum_{e=1}^{n_{el}} \int_{\Omega^e} \nabla \psi^h \, \nu_{\mathrm{DCID}} \nabla \varphi^h d\Omega = 0 \qquad (11)$$

Here n_{el} is the number of elements, τ_{SUPG} is the SUPG stabilization parameter [20], and ν_{DCID} is the discontinuity-capturing interface dissipation (DCID) proposed as:

$$\nu_{\mathrm{DCID}} = \frac{C_s}{2} h_{\mathrm{UGN}}^2 \sqrt{2 \boldsymbol{\varepsilon} : \boldsymbol{\varepsilon}} \frac{\left| \nabla \varphi^h \right| h_{\mathrm{UGN}}}{\varphi_{\mathrm{ref}}}, \qquad (12)$$

where C_s is a discontinuity-capturing parameter and φ_{ref} is a reference value set to 1. We note that the justification behind the expression given by Eq. (12) is combining some of the features we see in Eq. (7) and the discontinuity-capturing
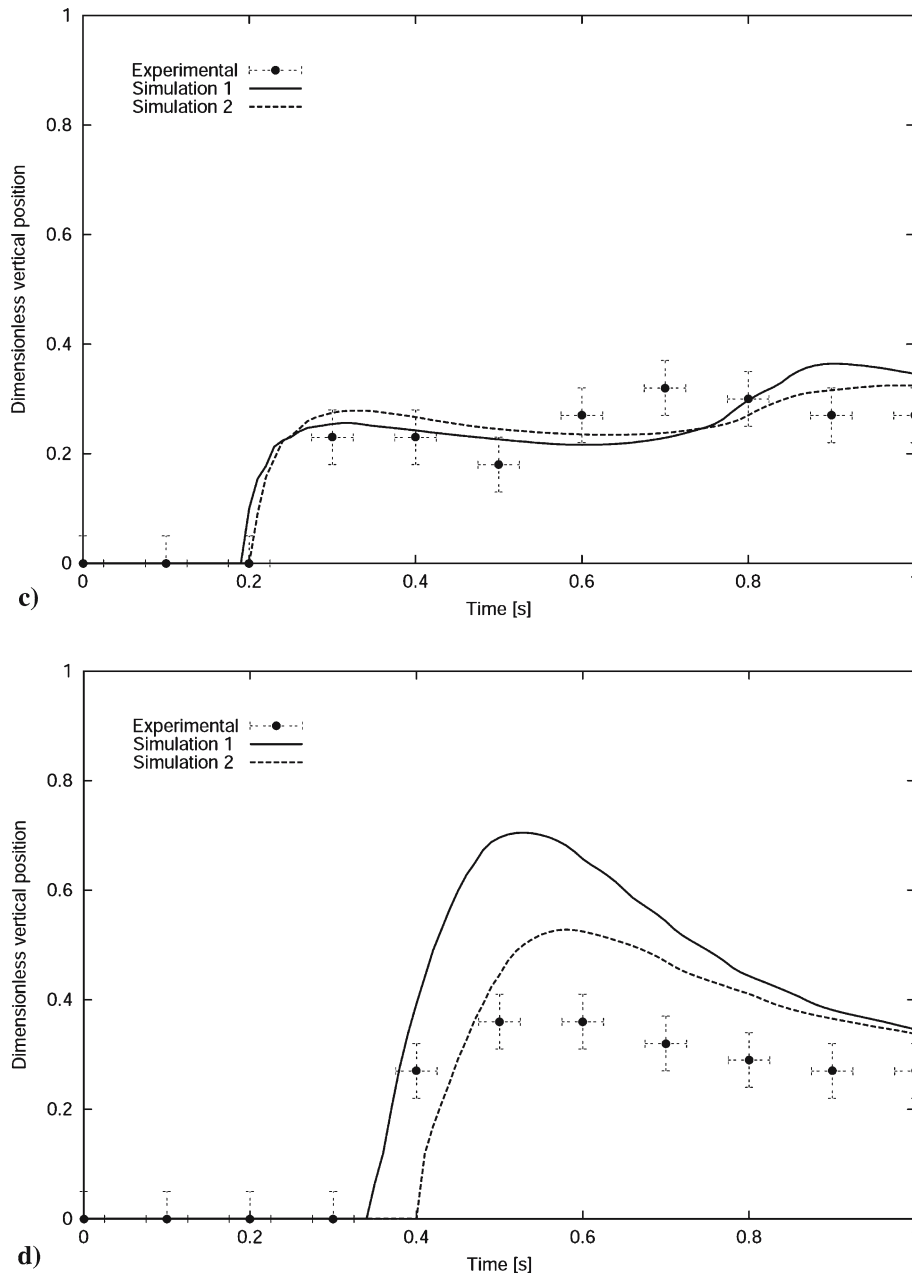
Fig. 5 (Contd.)

directional dissipation (DCDD) given in [20]. φ_{n+1}^h is computed from Eq. (11) by using a Crank–Nicholson time integration scheme.

From φ_{n+1}^h we obtain φ_{n+1}^{he} by a combination of a least-squares projection:

$$\int_\Omega \left(\psi_{n+1}^{he}\right)_P \left[(\varphi_{n+1}^{he})_P - \varphi_{n+1}^h\right] d\Omega = 0 \tag{13}$$

and corrections to enforce volume conservation for chunks of Fluids 1 and 2 [32]. The subscript P in Eq. (13) is used for representing the intermediate values following the projection, but prior to the corrections for the volume conservation.

In this technique, $(\varphi_{n+1}^{he})_P = H\left(\varphi_{n+1}^h - 0.5\right)$, where H is the Heaviside function. The volume conservation condition is given by the following equation:

$$\int_\Omega \left(\varphi_{n+1}^{he} - \varphi_n^{he}\right) d\Omega = Q, \tag{14}$$

where Q is the mass inflow/outflow in the time interval $[n, n+1]$. An iterative procedure is employed to satisfy Eq. (14). The mass balance ratio is defined as

$$R_m = \left[\int_\Omega (\varphi_{n+1}^{he} - \varphi_n^{he}) d\Omega\right] \bigg/ Q \quad \text{for } Q \neq 0, \tag{15}$$
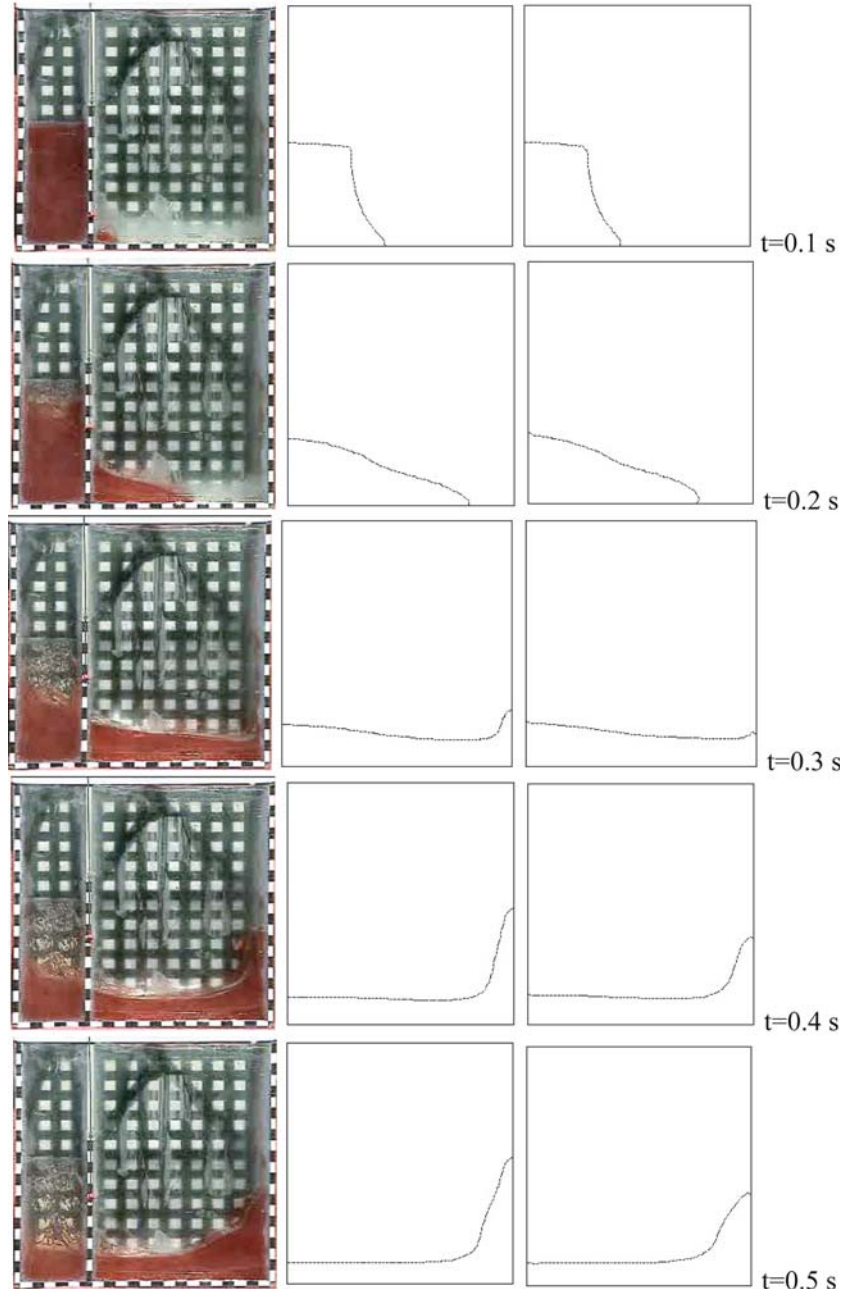
Fig. 6 Collapse of a shampoo column with aspect ratio $A_r = 2$. Interface positions at different instants: experimental (*left*) and numerical results computed without (Simulation 1, *middle*) and with (Simulation 2, *right*) wall friction effects

$$R_m = \left(\int_\Omega \varphi_{n+1}^{he} d\Omega \right) \Big/ \left(\int_\Omega \varphi_n^{he} d\Omega \right) \quad \text{for } Q = 0. \quad (16)$$

The residual R_m needs to be equal to 1.0 for volume conservation. To achieve this, φ_{n+1}^h is corrected iteratively as follows:

$$\varphi_{n+1,i+1}^h = \varphi_n^h + \left(\varphi_{n+1,i}^h - \varphi_n^h \right) / (R_m)^k, \quad (17)$$

where $k = \text{sign}\left(\varphi_{n+1,i}^h - \varphi_n^h \right)$ and i is the iteration counter. The iterations continue until the volume conservation condi-

tion is reached, i.e. $|R_m - 1.0| < \varepsilon_R$, where ε_R is an acceptable tolerance. When the convergence is reached, φ_{n+1}^h generates a volume-conserving value for φ_{n+1}^{he}. This value serves as the starting point for the computations in marching from $n + 1$ to $n + 2$.

4 Experimental procedure

The collapse of a water column was extensively studied in open channels [35] and in closed containers [11]. In the
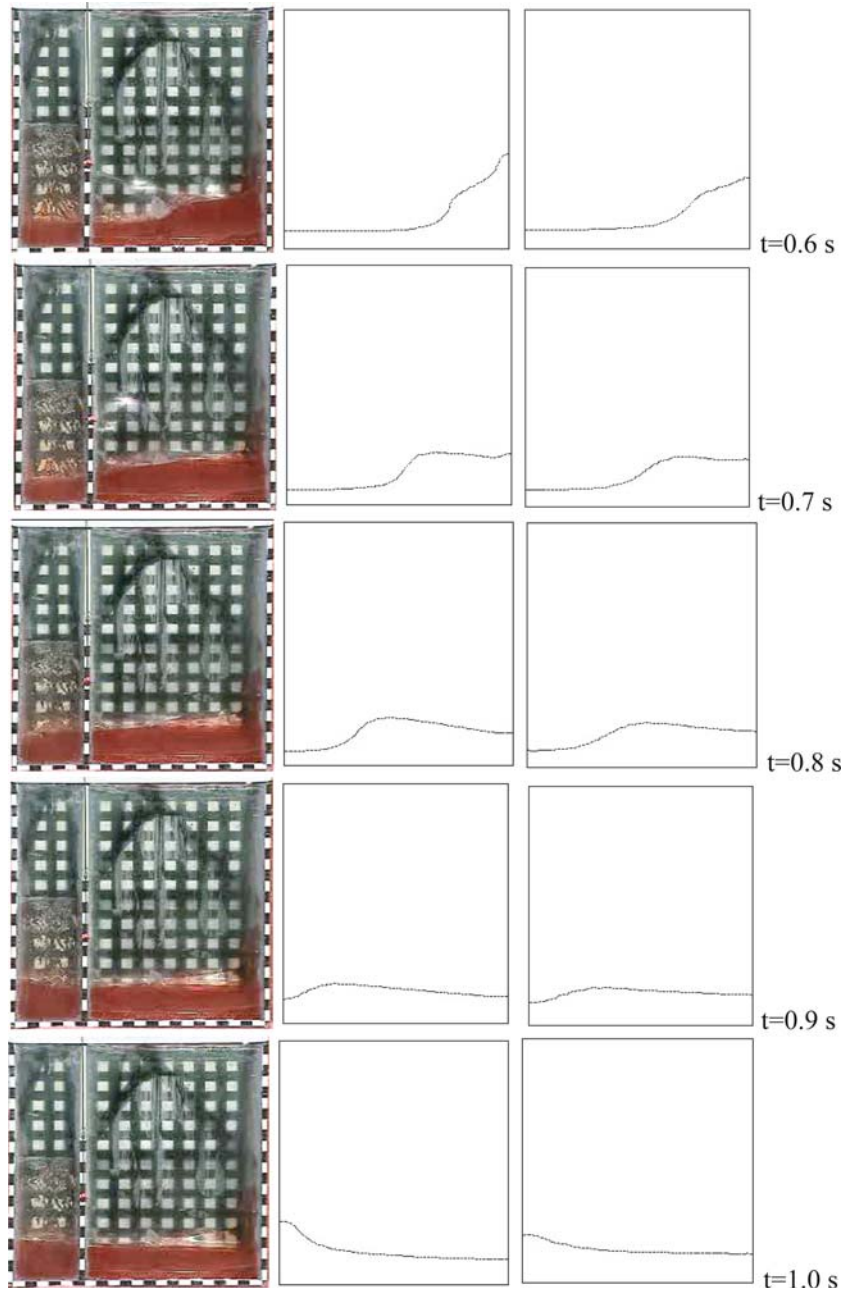
Fig. 6 (Contd.)

present work, a simple experimental setup was built to compare the experimental data with the numerical results to be evaluated in Sect. 5. The apparatus used is shown in Fig. 1 and consists of a glass box with two parts delimited by a gate with a mechanical release system. The left part of the box is initially filled with a liquid: shampoo or coloured water. In both cases two different liquid aspects ratios were tested: $A_r = 1$ and $A_r = 2$ ($A_r = H/L$, with H and L being the initial height and width of the column respectively, with $L = 0.114$ m).

Different experiments were carried out and recorded to a film. To measure the interface position, a ruler with tics 0.02 m apart is drawn surrounding the box and over the frame of the gate. A red marker that jointly moves with the gate helps to observe its position during the gate opening. The measurements reported in the present work are average values from the measurements registered for a minimum of five experiments. The maximum experimental errors in space and time are estimated as ± 0.005 m and ± 0.025 s, respectively.
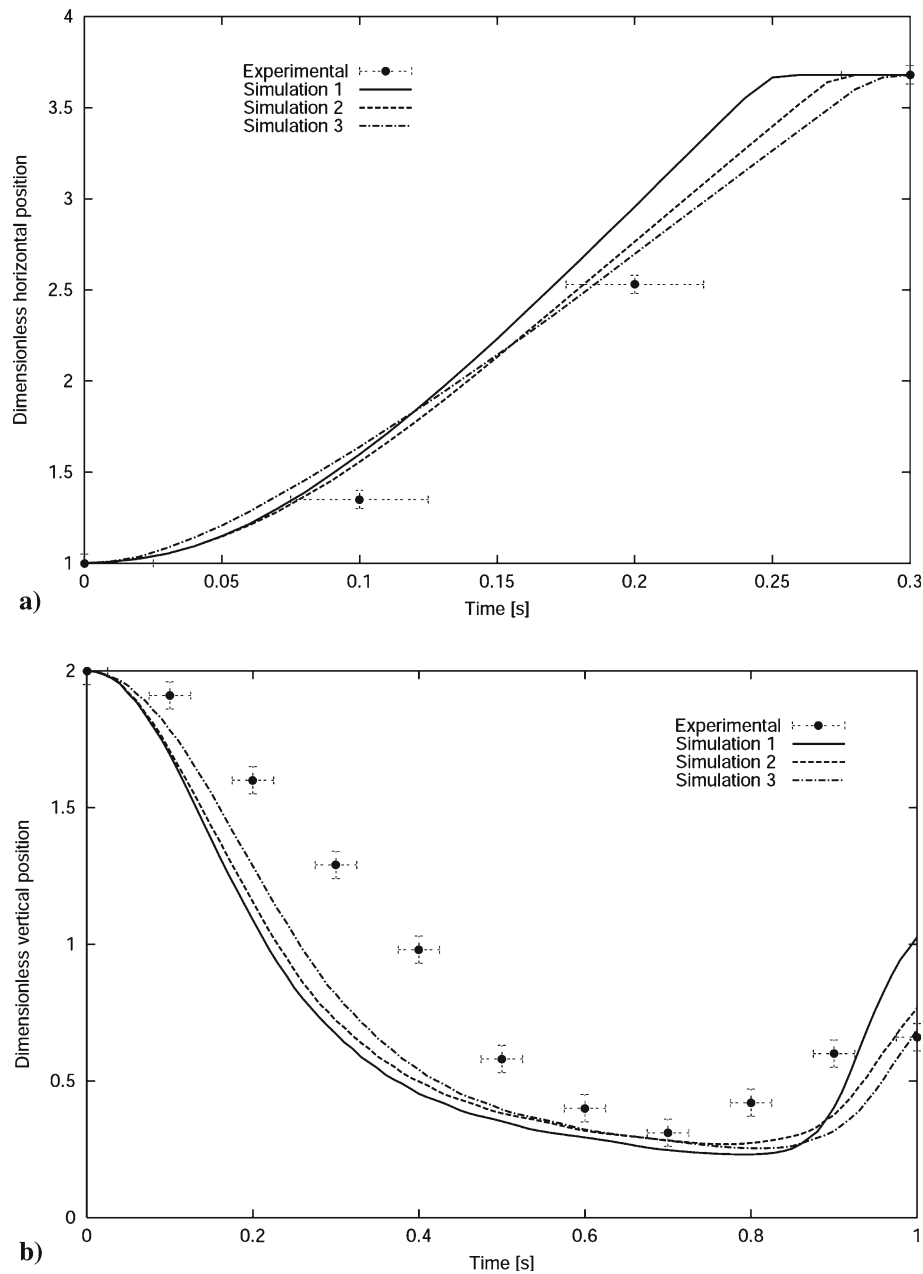
Fig. 7 Collapse of a shampoo column with aspect ratio $A_r = 2$: **a** dimensionless horizontal position (x/L) at $y = 0.0$ m (*bottom wall*), **b** dimensionless vertical position (y/L) at $x = 0.0$ m (*left wall*), **c** dimensionless vertical position (y/L) at $x = 0.27$ m (*middle of the box*) and **d** dimensionless vertical position (y/L) $x = 0.42$ m (*right wall*). Numerical results computed without (Simulation 1) and with (Simulation 2) wall friction effects. Simulation 3 was carried out with the wall friction effects and a finite gate opening speed

To evaluate the performance of the experimental procedure, the observed evolution of the interface at the bottom and left walls of the box are compared in Figs. 2 and 3 with those reported in [11] and [35], up to the instant that the liquid impinges on the right wall. The dimensionless horizontal position (x/L) at the bottom wall versus dimensionless time ($t[A_r g/L]^{1/2}$, with t being the real time and g the gravity modulus) is plotted in Figs. 2a and 3a for the two aspect ratios and both liquids. Figures 2b and 3b show for the same cases the evolution of the dimensionless vertical position (y/L) at the left wall (time scaled as in Figs. 2a and 3a). Figures 2 and 3 show that the measurements are in reasonably good agreement with those reported in the literature (in particular for water with $A_r = 2$). Note that the interface positions are delayed in time for the shampoo due to its higher viscosity.
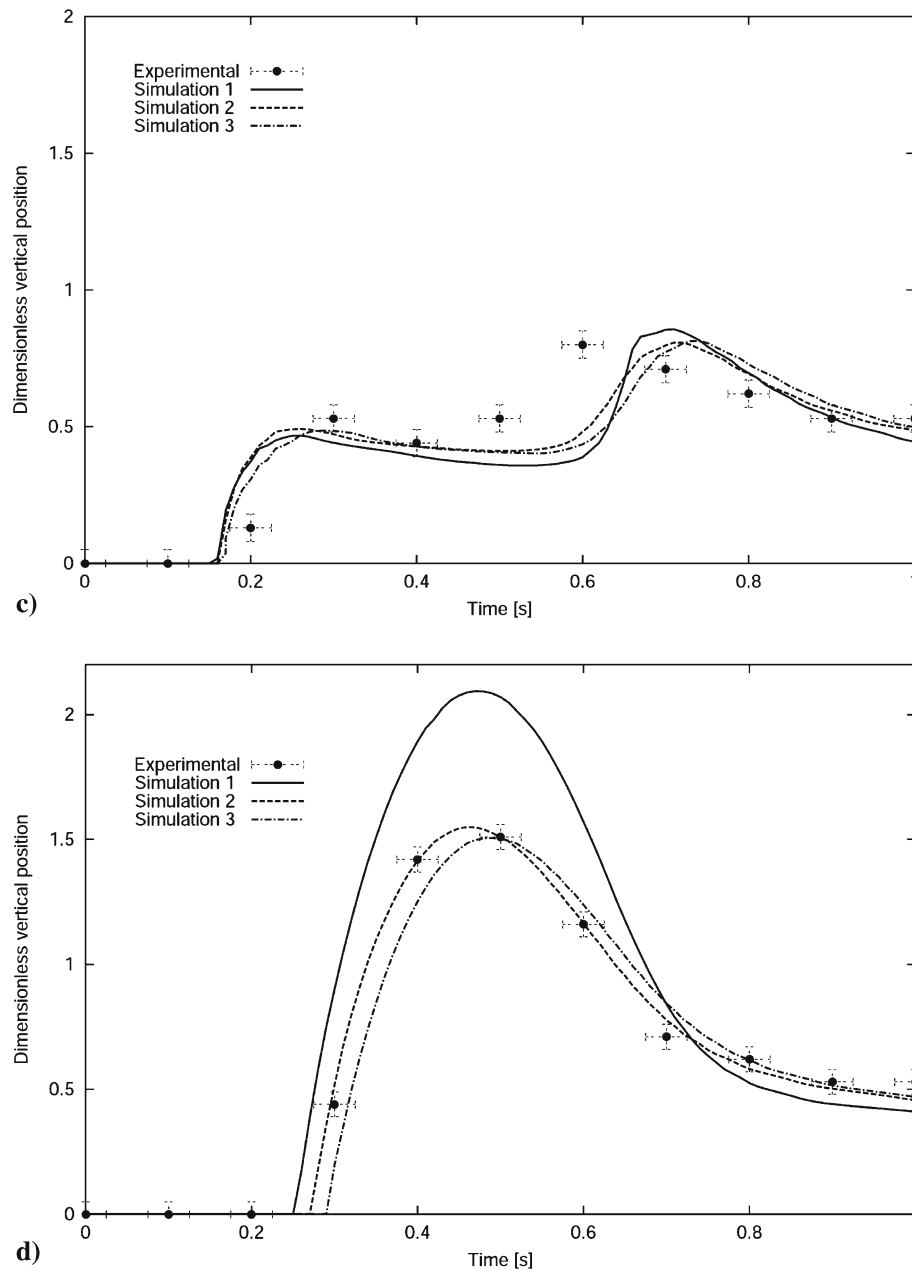
Fig. 7 (Contd.)

5 Comparison of numerical and experimental results

In [32] we discussed some performance aspects of the ETILT: sensitivity to mesh and time-step sizes, performance for structured and unstructured meshes, quadrilateral and triangular finite element discretizations, different sets of properties for the two liquids, and laminar and turbulent flow simulations. Also, in that a work the collapse of a water column was analyzed with a low value of the initial column width ($L = 0.05715$ m). The computed results, up to the instant of the water impingement on the right wall, were compared with those obtained using a Lagrangian technique and other numerical techniques and measurements reported in the literature.

In the present paper, the numerical simulations are focused on studying the long-term transient behavior for the collapse of a liquid column described in Sect. 4. In particular, the effects of the parameters used in modeling some of the physical aspects (wall friction and turbulence) as proposed in Sect. 3 are evaluated by comparing them with the experimental results. The influence of the DCID is also analyzed. In the simulations, the liquid column is initially at rest and confined
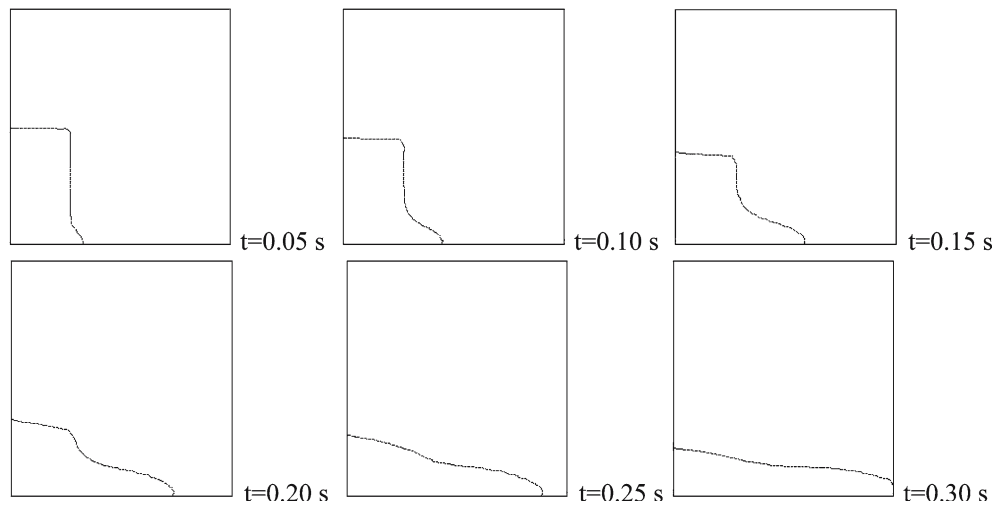
Fig. 8 Collapse of a shampoo column with aspect ratio $A_r = 2$. Interface positions at different instants: effect of the gate opening
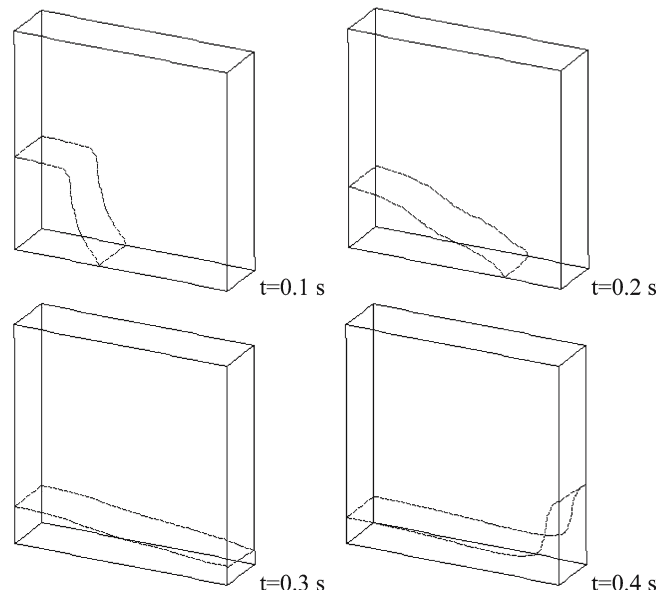

Fig. 9 Collapse of a shampoo column with aspect ratio $A_r = 2$. Interface positions at different instants: 3D analysis

between the left wall and the gate. The pressure is set to zero at the top of the rectangular computational domain.

5.1 Collapse of a shampoo column

The fluid properties are: $\rho_1 = 1,042$ kg/m^3 and $\mu_1 = 8$ kg/m/s for the shampoo (measured at a laboratory using a standard procedure), and $\rho_2 = 1$ kg/m^3 and $\mu_2 = 0.001$ kg/m/s for the air (lower values for the air viscosity do not play a significant role in the numerical predictions, as observed in [32]).

As the shampoo-glass contact effects are observed in experiments, simulations with slip (Simulation 1) and fric-

tion (Simulation 2) conditions at the walls were carried out to assess the influence of this effect on the interface response. In Simulation 2, we set $C_f = 190$ [see Eq. (6)] based on the numerical tests described below. A mesh composed of 60×45 four-noded isoparametric elements is used with a time-step size of 0.001 s.

Column of aspect ratio $A_r = 1$ Figure 4 shows the experimental interface positions at various instants together with the corresponding predictions computed via Simulations 1 and 2. A detailed description of the interface evolution is shown in Fig. 5.
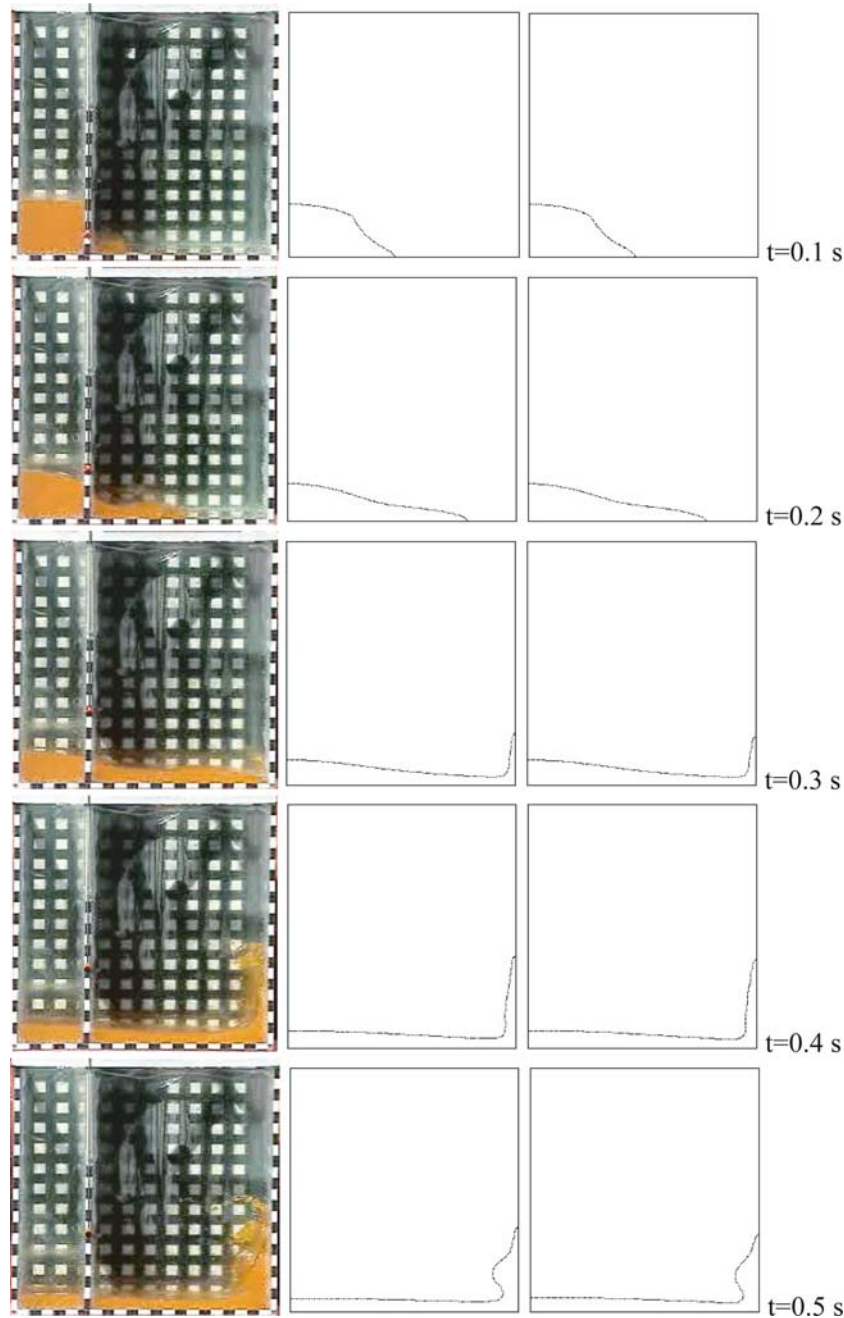
Fig. 10 Collapse of a water column with aspect ratio $A_r = 1$. Interface positions at different instants: experimental (*left*) and numerical results computed without (Simulation 1, *middle*) and with (Simulation 2, *right*) discontinuity-capturing dissipation

The interface evolution at the bottom of the box during the spread of the liquid under the gravity is plotted in Fig. 5a up to the instant when the shampoo interface reaches the right wall ($t \approx 0.4$ s). The motion of the horizontal position of the interface is delayed due to the wall friction effects.

The time histories for the vertical position at the left wall, middle of the box and right wall are shown in Figs. 5b, c and d. From these figures, it is apparent that, in the experiment, the

shampoo motion practically stops once the interface impinges on the right wall. Although similar predictions of the interface vertical position at the left wall are obtained for Simulations 1 and 2, some differences with the experimental results persist. As can be seen, the maximum interface vertical position at the middle of the box is captured reasonably well in the simulations, but the results exhibit a time delay. With the friction wall model, the maximum value of the interface vertical position at the right wall is reduced. Nevertheless,
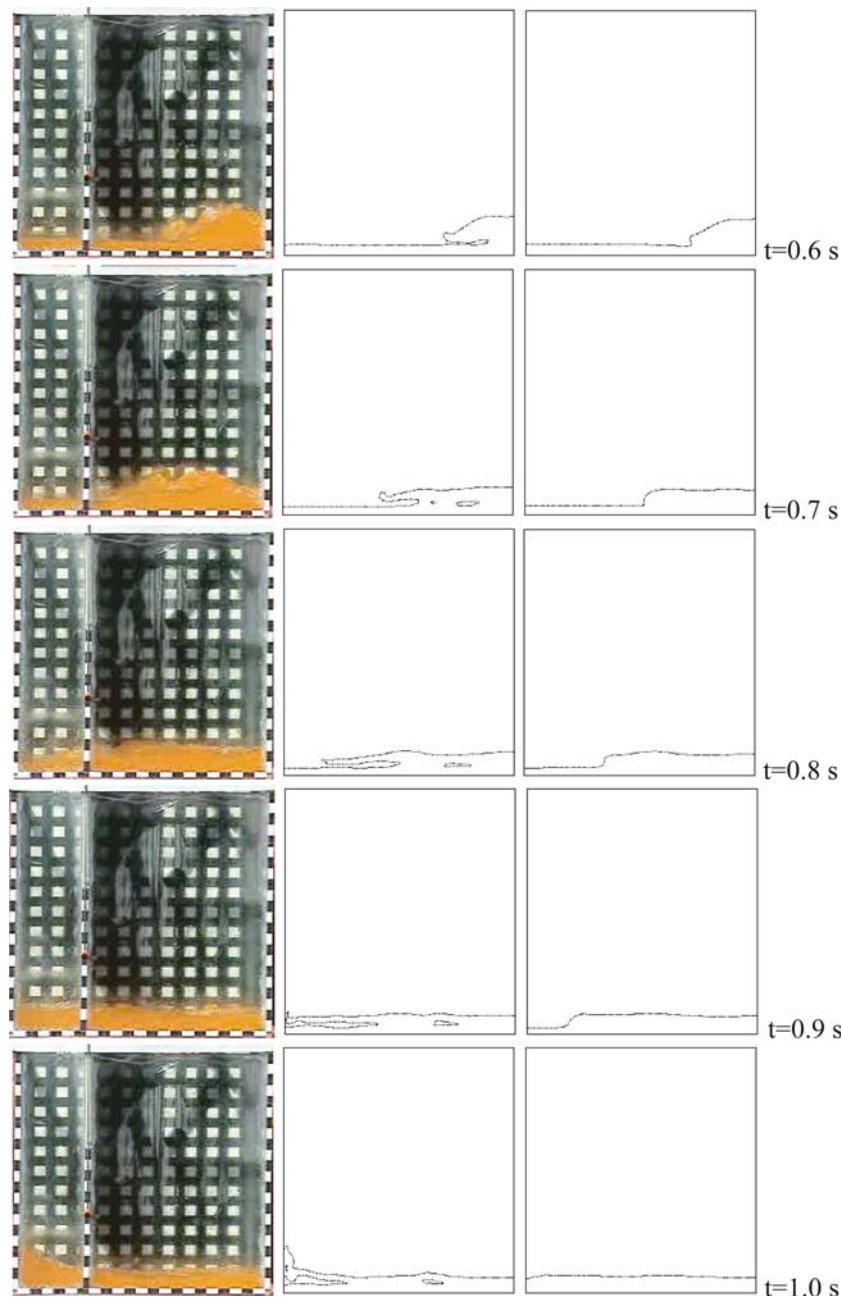
Fig. 10 (Contd.)

Fig. 5 shows that the overall trends for the interface behavior are captured reasonably well.

Column of aspect ratio $A_r = 2$ Figure 6 shows the experimental interface positions at different instants and the numerical results obtained with Simulations 1 and 2.

To evaluate the effect of the gate opening, an additional computation is carried out with the gate not opening instantaneously but with a finite speed (Simulation 3). The gate opening speed was extracted from the experiments. In this simulation, an average gate opening speed of 0.86 m/s is used,

while the friction conditions are used on both the walls and the gate.

Evolutions of the horizontal position of the interface at the bottom of the box and the vertical position at the left wall, middle of the box and right wall are shown in Fig. 7 together with the experimental results.

The simulations show that the interface, as it was also observed in the experiments, still moves after the first impingement on the right wall ($t \approx 0.3$ s). The reflected wave realistically represents the real liquid motion. The results computed with Simulation 2 satisfactorily capture the
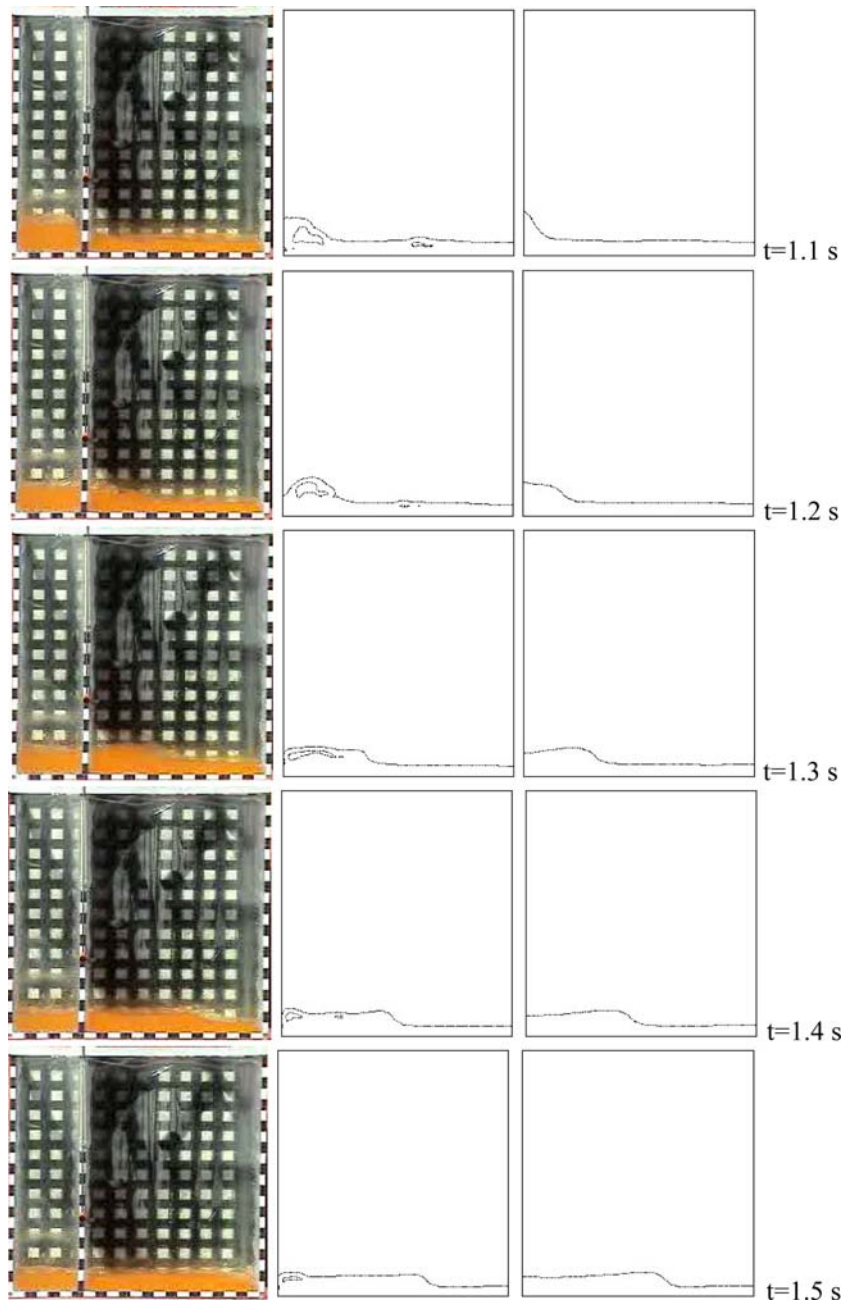
Fig. 10 (Contd.)

maximum and minimum interface vertical positions and the time of the first impingement on the right wall.

The gate opening effect included in Simulation 3 slightly changes the results obtained in Simulation 2. With the gate opening effect, more advanced interface positions at early instants of the analysis are obtained at the bottom of the box. This is due to the "orifice effect" induced at the beginning of the gate opening, which increases the velocity at the bottom of the box. This situation quickly changes and the liquid

attaches to the right wall later than it does in Simulation 2. The interface positions at different instants obtained with Simulation 3 are shown in Fig. 8.

In the present study, numerical analyses with different values of the friction coefficient C_f were carried out for the shampoo columns with aspect ratios 1 and 2 (results not shown). The value $C_f = 190$ was selected on the basis that it leads to minimum differences between the numerical predictions of the interface position and the corresponding
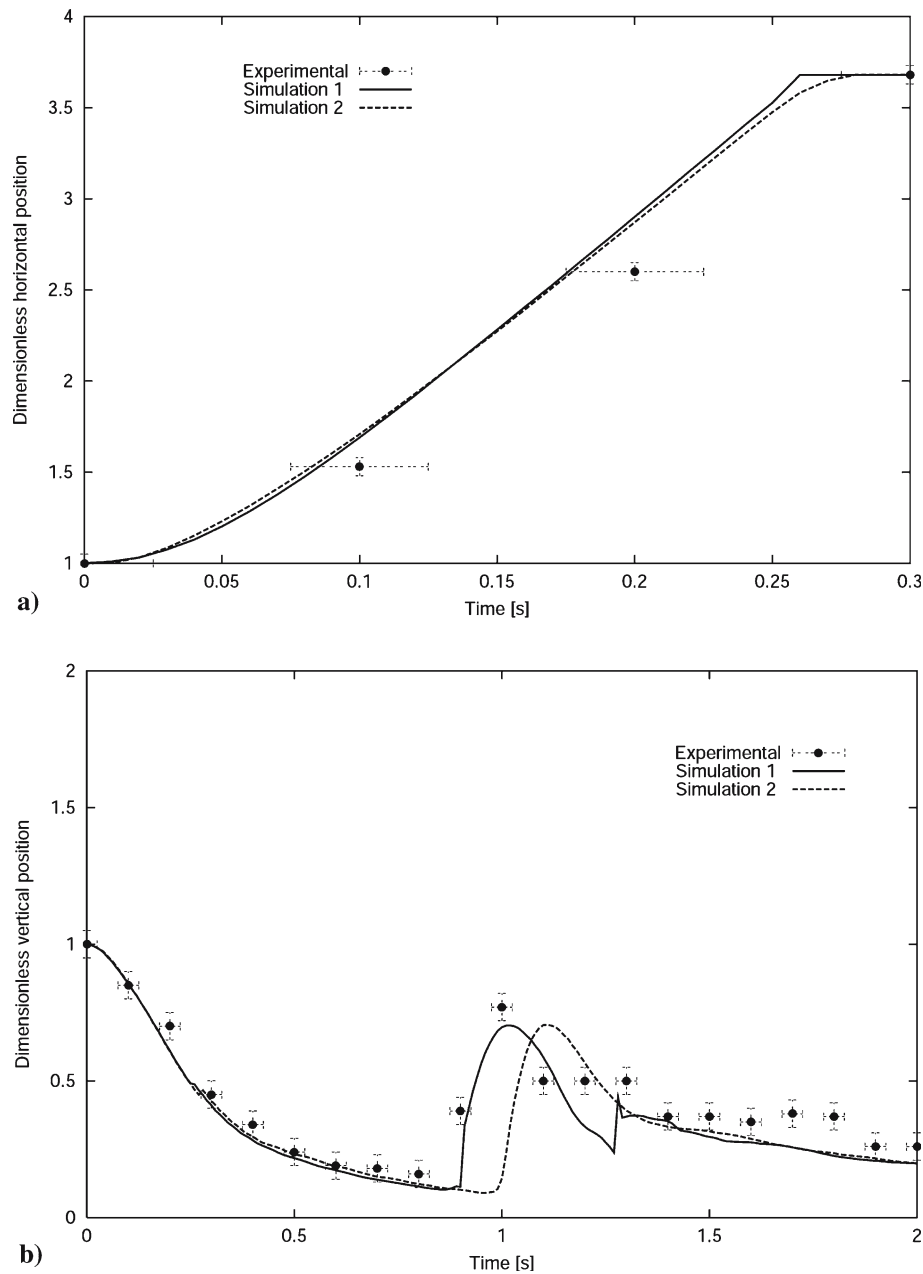
Fig. 11 Collapse of a water column with aspect ratio $A_r = 1$: **a** dimensionless horizontal position (x/L) at $y = 0.0$ m (*bottom wall*), **b** dimensionless vertical position (y/L) at $x = 0.0$ m (*left wall*), **c** dimensionless vertical position (y/L) at $x = 0.27$ m (*middle of the box*) and **d** dimensionless vertical position (y/L) at $x = 0.42$ m (*right wall*). Numerical results computed without (Simulation 1) and with (Simulation 2) discontinuity-capturing dissipation

measurements. Such differences can not be fully eliminated with just a friction model, because other aspects, such as surface tension (not included in the model), should also play a role.

In the computations reported above, the shampoo was considered a Newtonian fluid. A more realistic representation of the material behavior for the shampoo can be based on choosing a viscosity that decreases with the increasing shear rate. To evaluate this effect, an additional computation was carried out using a simple constitutive model based on the power law of the shear rate. The preliminary results (not shown) did not show any quantitative changes.

We also carried out a 3D computation based on the conditions of Simulation 1. These results are included to briefly assess the performance of the proposed technique in a 3D case. The interface position is shown in Fig. 9, and we see that the interface evolution is close to what we obtained in the 2D analysis. This trend agrees with the fact that 3D effects were not observed in the experiments.
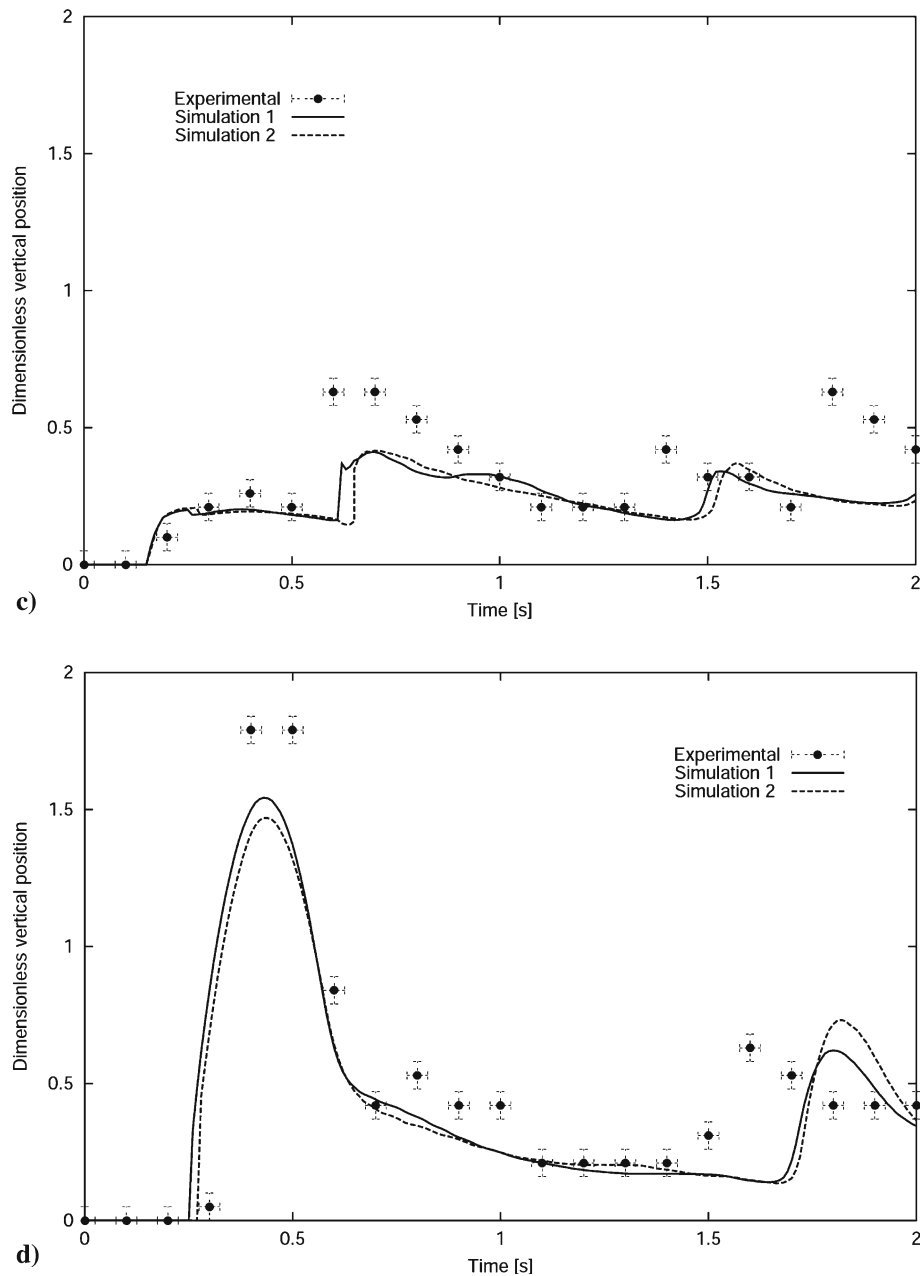
Fig. 11 (Contd.)

5.2 Collapse of a water column

In this case the gate is assumed to be suddenly removed at time $t = 0$ s. Slip conditions are assumed at the solid surfaces. The fluid properties are: $\rho_1 = 1,000\,\mathrm{kg/m^3}$ and $\mu_1 = 0.001\,\mathrm{kg/m/s}$ for the water, and $\rho_2 = 1\,\mathrm{kg/m^3}$ and $\mu_2 = 0.001\,\mathrm{kg/m/s}$ for the air.

Two simulations are carried out: Simulations 1 and 2. Both simulations include a simple turbulence model (defined by Eq. (7) and with $C_t = 3.57$). Simulation 2 also has the DCID (defined by Eq. (12) and with $C_s = 10$). The value

of the coefficient C_s was selected from numerical tests by trying to minimize the differences between the numerical predictions and the experimental measurements for both aspect ratios.

The mesh is composed of 100×75 four-noded isoparametric elements. The time-step size is 0.001 s.

Column of aspect ratio $A_r = 1$ The experimental and numerical interface positions at various instants are shown in Fig. 10. The cut-off value of the viscosity in Eq. (7) is set as $\mu_{\max} = 1.5\,\mathrm{kg/m/s}$. In the experiments, it is observed that
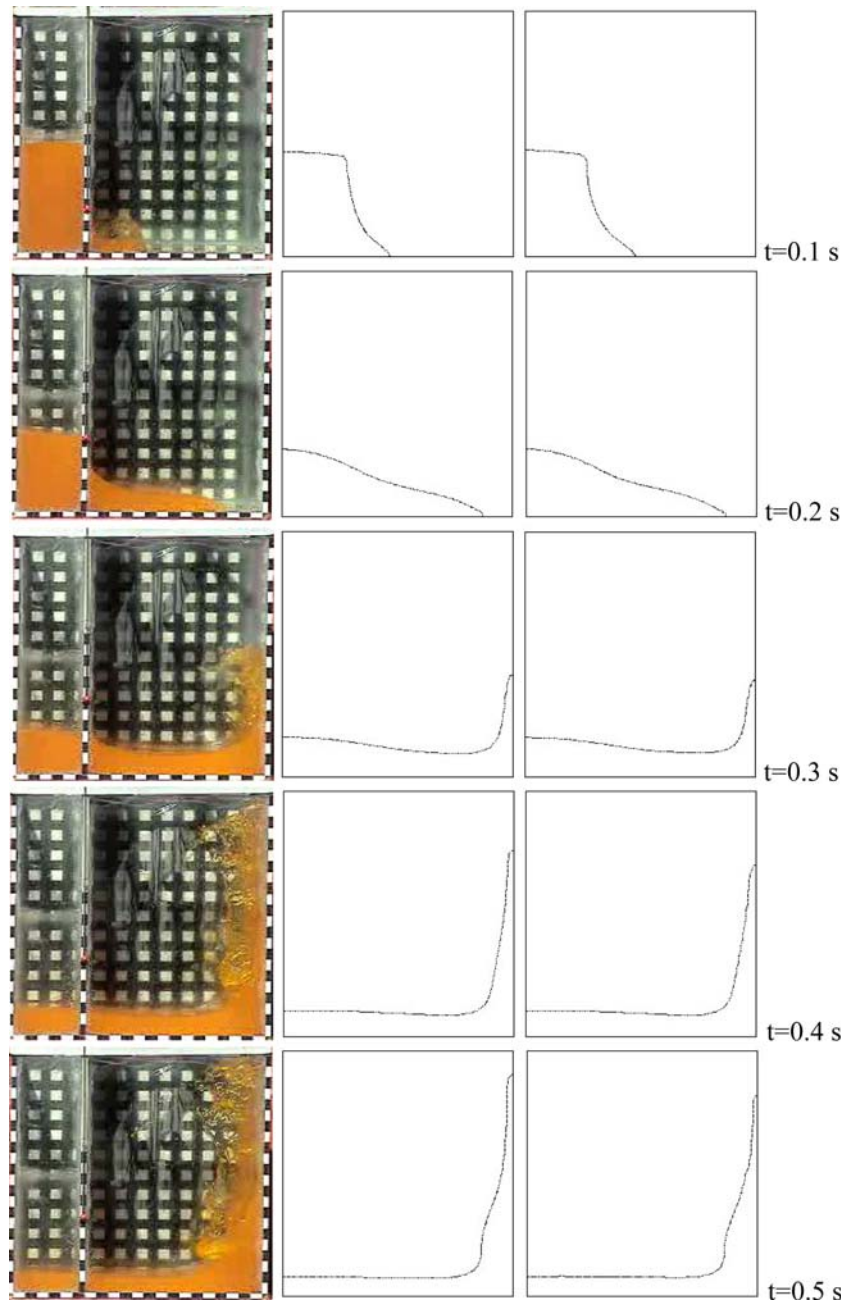
Fig. 12 Collapse of a water column with aspect ratio $A_r = 2$. Interface positions at different instants: experimental (*left*) and numerical results computed without (Simulation 1, *middle*) and with (Simulation 2, *right*) discontinuity-capturing dissipation

separated flows are developed close to the interface at specific instants (e.g., during the liquid impingement on the walls). The separated fluid quickly merges with the bulk liquid and no bubbles are seen. However, bubbles are obtained in Simulation 1 for $t \geq 0.6$ s. Although they are caused due to the folding of the interface, they have no physical meaning beyond that. Note that the formulation does not include a bubble model. When the DCID is activated (Simulation 2), the formation of bubbles in the bulk liquid are inhibited and the interface is represented as a continuous front.

Figure 11 shows, for the experiments and Simulations 1 and 2, the evolutions of the interface horizontal position at the bottom of the box and the interface vertical position at the left wall, middle of the box and right wall. The results are in reasonably good agreement with the experimental data. The computed vertical position of the interface at the left wall practically coincides with the experimental results up to $t = 0.9$ s. Additionally, the magnitude of its second maximum is well described. The numerical behavior of the interface vertical position at the middle of the box also shows good
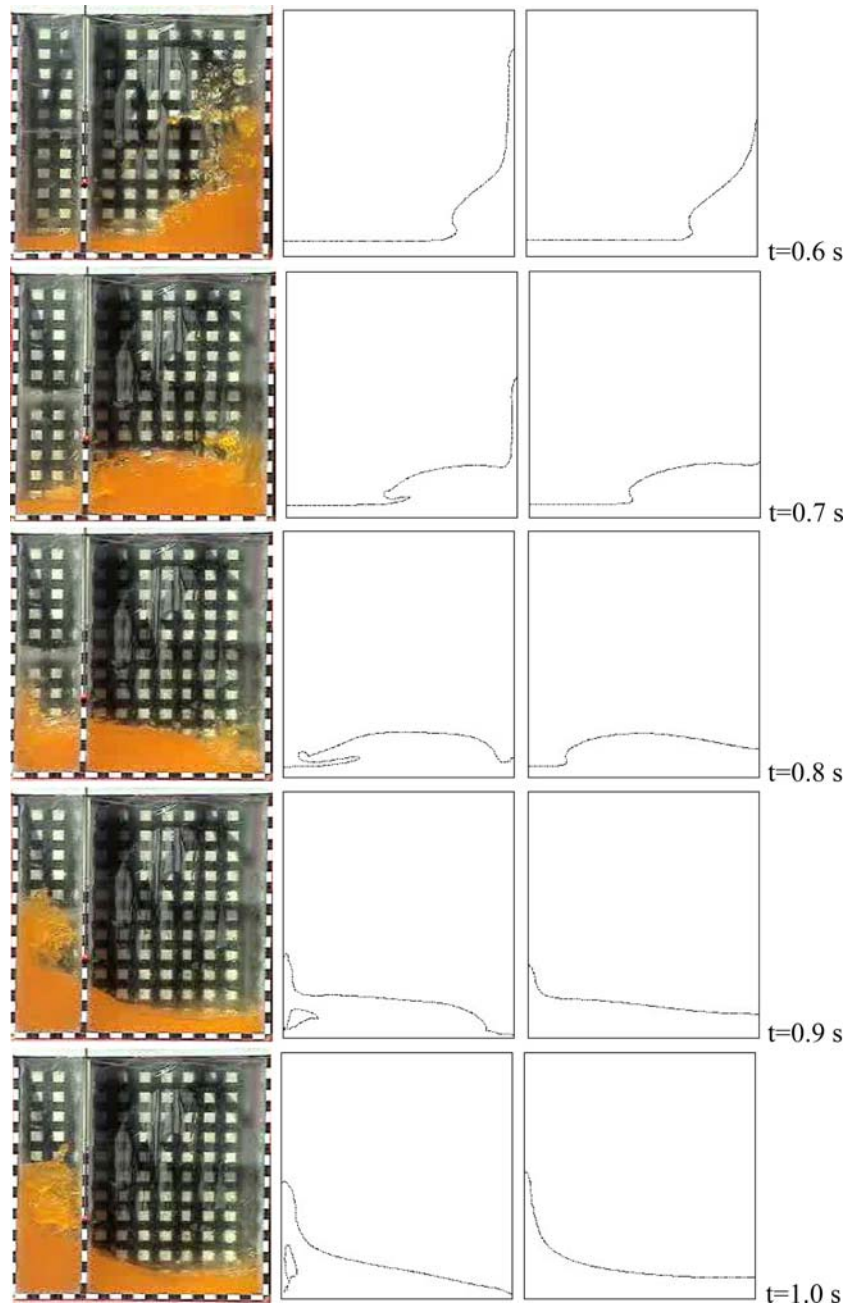
Fig. 12 (Contd.)

agreement between the numerical and experimental results up to $t = 0.6$ s. After that, we see some discrepancies in the maximum values and a delay in the occurrence of the second maximum. The computed vertical interface position at the right wall captures reasonably well the instant of the first impingement ($t = 0.25$ s) and first maximum ($t = 0.45$ s). The maximum value, however, is lower than that observed experimentally. The second maximum is described reasonably well in magnitude but has a delayed time.

Column of aspect ratio $A_r = 2$ In this case $\mu_{max} = 3.0$ kg/m/s. Figure 12 shows the interface positions at various instants. The time history of the interface horizontal position along the bottom of the box and the interface vertical position at selected locations are shown in Fig. 13.

The numerical results obtained in this case show trends that are similar to those observed in the previous analysis. In particular, the numerical evolutions of the interface positions at the bottom of the box and along the left wall
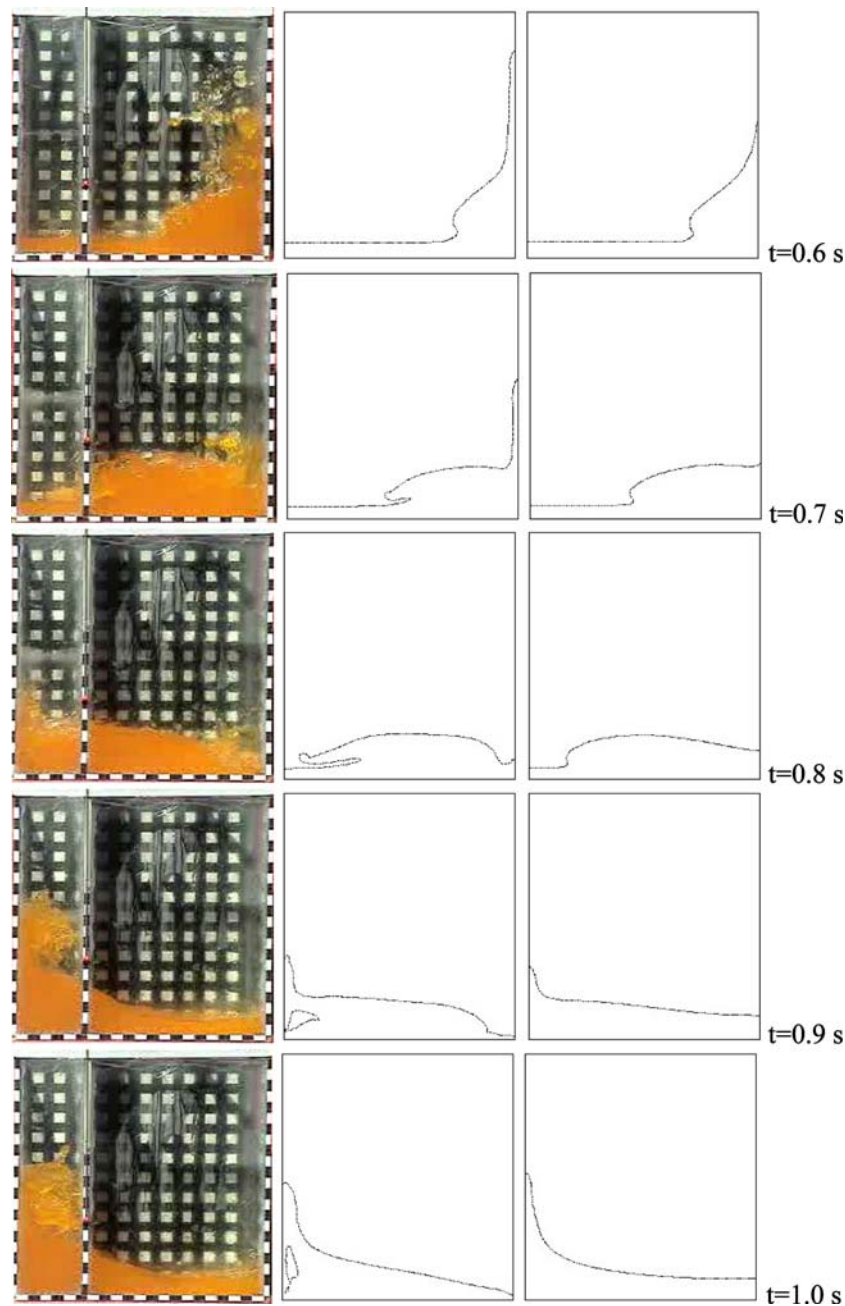
Fig. 12 (Contd.)

satisfactorily match the corresponding measurements up to $t = 1.5$ s. Moreover, the time of the first impingement on the right wall is captured well. The amplitude of the reflected wave is predicted reasonably well but has a delayed time.

6 Conclusions

The performance of the ETILT was assessed in simulation of the collapse of liquid columns. A set of experiments have been carried out to obtain the evolution of the interface position. Two different fluids, shampoo and water, and two different column aspect ratios, 1 and 2, were studied.

Simple concepts were included in the model to describe the wall friction and turbulence effects in the analyses of the shampoo and water, respectively. Additionally, the influence of some proposed stabilization parameters was assessed.

The wall friction effect is particularly apparent in the collapse of the shampoo column due to its high viscosity.
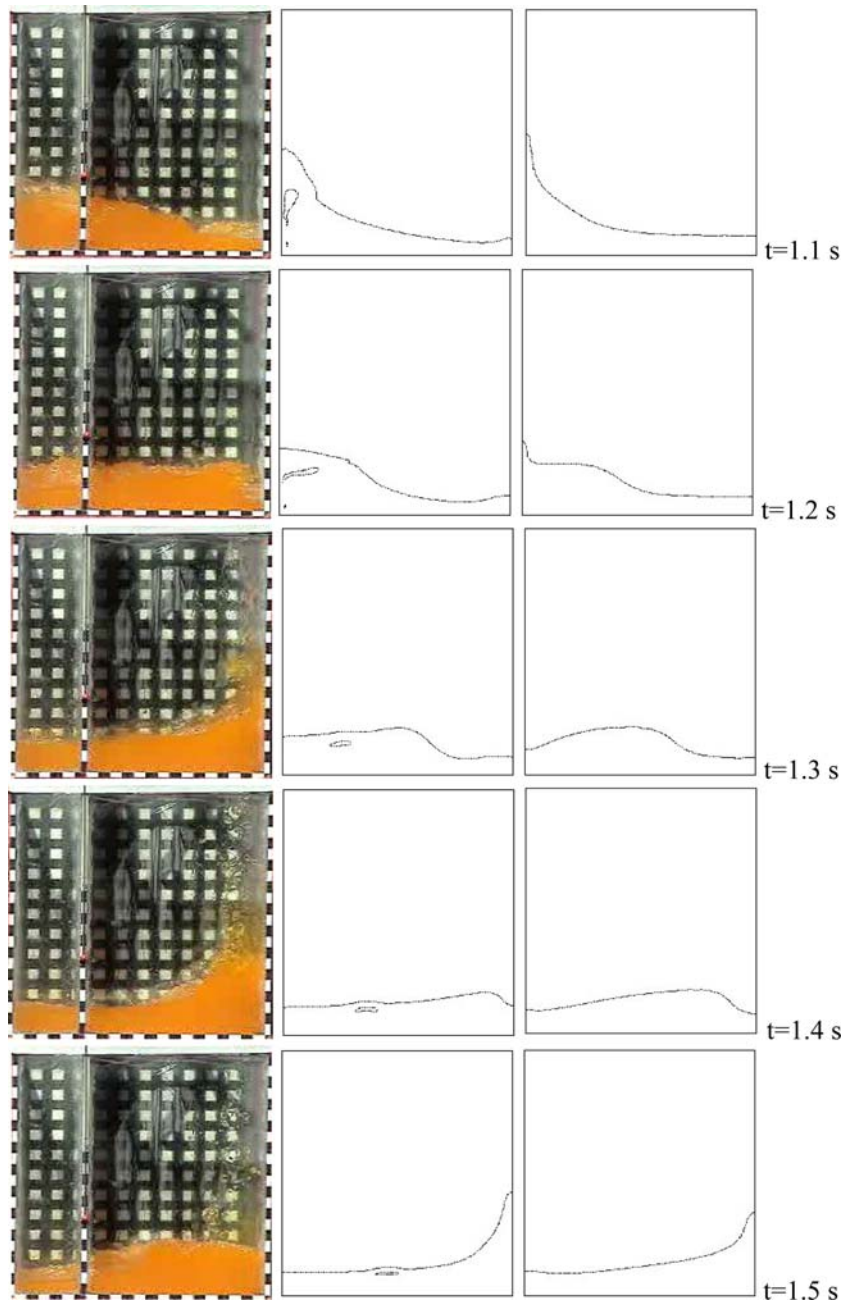
Fig. 12 (Contd.)

No separated flow was observed in the experiments. This aspect was also seen in the simulations where neither turbulence model nor discontinuity-capturing dissipation was used. The effect of the gate opening was found not to change the overall behavior of the interface. In addition, the 3D analysis provides results similar to those computed under the 2D assumption.

In the case of the collapse of the water column, since it is practically an inviscid fluid, the friction wall effect does not play much role in the analyses. No special model was included to represent the bubbles. Hence, once the bubbles are generated, the interface becomes unrealistic. The discontinuity-capturing dissipation included in the formulation helps to model the overall interface behavior reasonably well and inhibits the bubble formation in the bulk liquid. The turbulence model controls the height of the liquid columns on the walls and the wave evolution. A high mesh refinement is required to better represent the turbulence effects, and
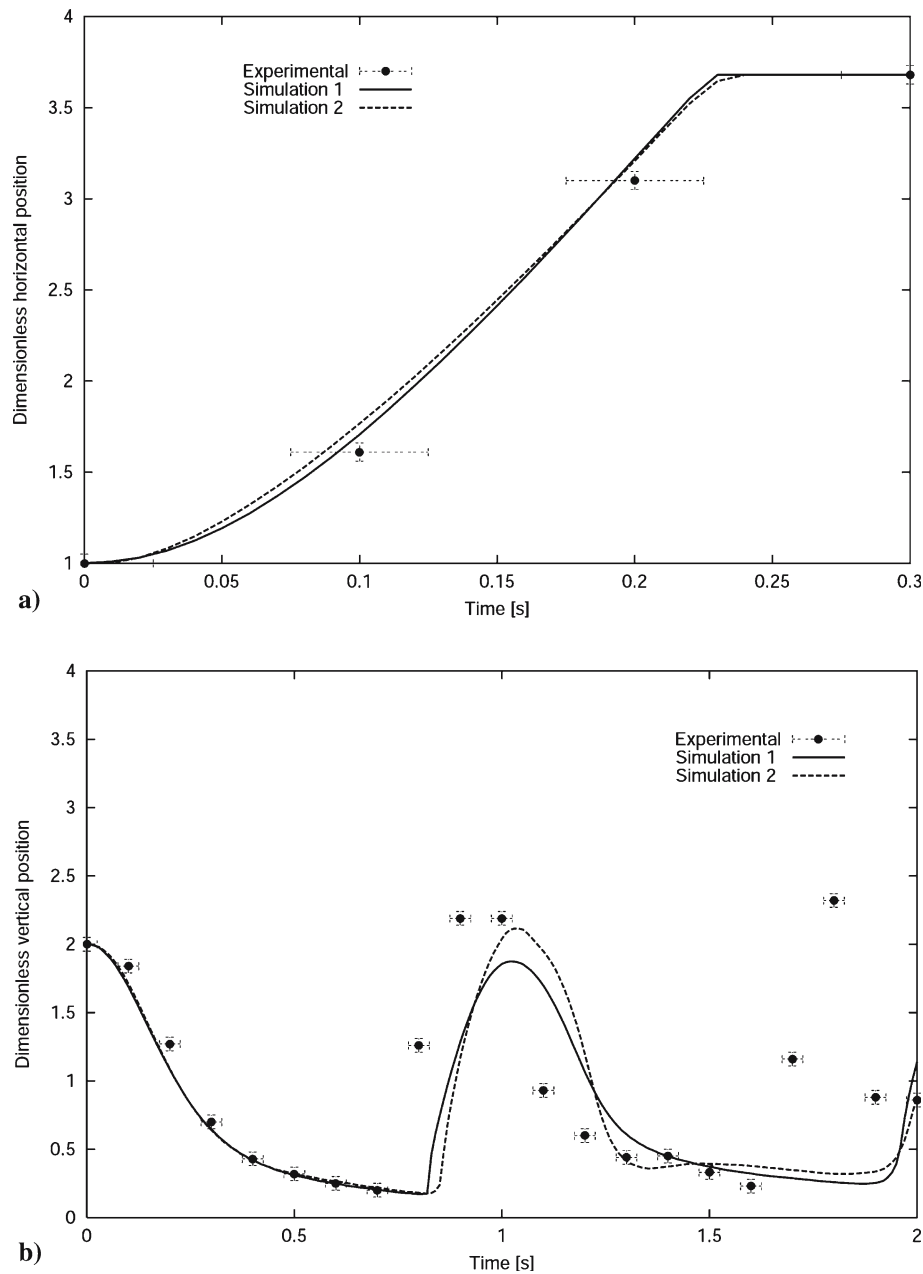
Fig. 13 Collapse of a water column with aspect ratio $A_r = 2$: **a** dimensionless horizontal position (x/L) at $y = 0.0$ m (*bottom wall*), **b** dimensionless vertical position (y/L) at $x = 0.0$ m (*left wall*), **c** dimensionless vertical position (y/L) at $x = 0.27$ m (*middle of the box*) and **d** dimensionless vertical position (y/L) at $x = 0.42$ m (*right wall*). Numerical results computed without (Simulation 1) and with (Simulation 2) discontinuity-capturing dissipation

reasonable results are obtained with the coefficients used in the turbulence model.

Overall, the numerical results compare satisfactorily with the measurements.
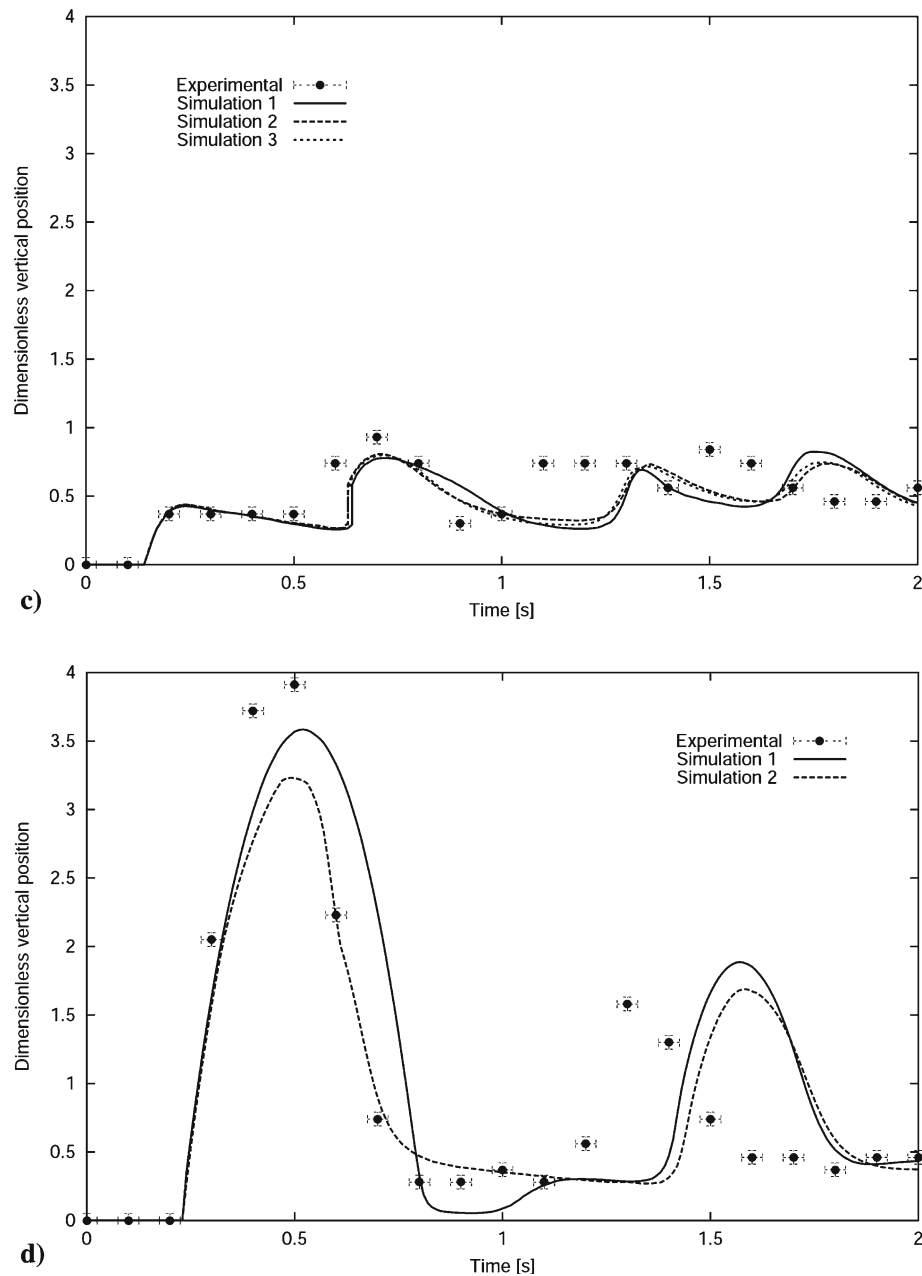
Fig. 13 (Contd.)

References

1. Brooks AN, Hughes TJR (1982) Streamline upwind/Petrov–Galerkin formulations for convection dominated flows with particular emphasis on the incompressible Navier–Stokes equations. Comput Methods Appl Mech Eng 32:199–259
2. Hughes TJR, Liu WK, Zimmermann TK (1981) Lagrangian-Eulerian finite element formulation for incompressible viscous flows. Comput Methods Appl Mech Eng 29:239–349
3. Liu WK (1981) Finite element procedures for fluid-structure interactions and application to liquid storage tanks. Nucl Eng Des 65:221–238
4. Huerta A, Liu W (1988) Viscous flow with large free surface motion. Comput Methods Appl Mech Eng 69:277–324
5. Tezduyar TE (1992) Stabilized finite element formulations for incompressible flow computations. Adv Appl Mech 28:1–44
6. Tezduyar TE, Behr M, Liu J (1992) A new strategy for finite element computations involving moving boundaries and interfaces – the deforming-spatial-domain/space-time procedure: I. The concept and the preliminary numerical tests. Comput Methods Appl Mech Eng 94:339–351
7. Tezduyar TE, Behr M, Mittal S, Liu J (1992) A new strategy for finite element computations involving moving boundaries and interfaces – the deforming-spatial-domain/space-time procedure: II. Computation of free-surfaces flows, two-liquid flows, and flows

with drifting cylinders. Comput Methods Appl Mech Eng 94:353–371

8. Braess H, Wriggers P (2000) Arbitrary Lagrangian–Eulerian finite element analysis of free surface flow. Comput Methods Appl Mech Eng 190:95–109

9. Feng YT, Perić D (2003) A spatially adaptive linear space-time finite element solution procedure for incompressible flows with moving domains. Int J Numer Methods Fluids 43:1099–1106

10. Rabier S, Medale M (2003) Computation of free surface flows with a projection FEM in a moving mesh framework. Comput Methods Appl Mech Eng 192:4703–4721

11. Koshizuka S, Oka Y (1996) Moving-particle semi-implicit method for fragmentation of incompressible fluid. Nucl Sci Eng 123:421–434

12. Bonet J, Kulasegaram S, Rodriguez-Paz MX, Profit M (2004) Variational formulation for the smooth particle hydrodynamics (SPH) simulation of fluid and solid problems. Comput Methods Appl Mech Eng 193:928–948

13. Kulasegaram S, Bonet J, Lewis RW, Profit M (2004) A variational formulation based contact algorithm for rigid boundaries in two-dimensional SPH applications. Comput Mech 33:316–325

14. Xie H, Koshizuka S, Oka Y (2004) Modelling of a single drop impact onto liquid film using particle method. Int J Numer Methods Fluids 45:1009–1023

15. Idelsohn S, Storti M, Oñate E (2003) A Lagrangian meshless finite element method applied to fluid-structure interaction problems. Comput Struct 81:655–671

16. Tezduyar T, Aliabadi S, Behr M (1998) Enhanced-discretization interface-capturing technique (EDICT) for computation of unsteady flows with interfaces. Comput Methods Appl Mech Eng 155:235–248

17. Osher S, Fedkiw P (2001) Level set methods: and overview and some recent results. J Comput Phys 169:463–502

18. Sethian JA (2001) Evolution, implementation, and application of level set and fast marching methods for advancing fronts. J Comput Phys 169:503–555

19. Tezduyar TE (2001) Finite element methods for flow problems with moving boundaries and interfaces. Arch Comput Methods Eng 8:83–130

20. Tezduyar TE (2003) Computation of moving boundaries and interfaces and stabilization parameters. Int J Numer Methods Fluids 43:555–575

21. Kim MS, Lee WI (2003) A new VOF-based numerical scheme for the simulation of fluid flow with free surface. Part I: New free surface-tracking algorithm and its verification. Int J Numer Methods Fluids 42:765–790

22. Minev P, Chen T, Nandakumar K (2003) A finite element technique for multifluid incompressible flow using Eulerian grids. J Comput Phys 187:255–273

23. Sochnikov V, Efrima S (2003) Level set calculations of the evolution of boundaries on a dynamically adaptive grid. Int J Numer Methods Eng 56:1913–1929

24. Yue W, Lin CL, Patel VC (2003) Numerical simulation of unsteady multidimensional free surface motons by level set method. Int J Numer Methods Fluids 42:853–884

25. Tezduyar TE, Sathe S (2004) Enhanced-discretization space-time technique (EDSTT). Comput Methods Appl Mech Eng 193:1385–1401

26. Kohno H, Tanahashi T (2004) Numerical analysis of moving interfaces using a level set method coupled with adaptive mesh refinement. Int J Numer Methods Fluids 45:921–944

27. Wang JP, Borthwick AGL, Taylor RE (2004) Finite-volume-type VOF method on dynamically adaptive quadtree grids. Int J Numer Methods Fluids 45:485–508

28. Greaves D (2004) Simulation of interface and free surface flows in a viscous fluid using adapting quadtree grids. Int J Numer Methods Fluids 44:1093–1117

29. Cruchaga MA, Celentano DJ, Tezduyar TE (2004) Modeling of moving interface problems with the ETILT. In: Computational mechanics proceedings of the WCCM VI in conjunction with AP-COM'04. Tsinghua University Press and Spring-Verlag, Beijing, China

30. Tezduyar TE (2004) Finite elements methods for fluid dynamics with moving boundaries and interfaces. In: Stein E, De Borts R, Hughes TJR (eds) Encyclopedia of computational mechanics, Fluids, vol 3, chapt 17. Wiley, New York

31. Tezduyar TE (2004) Moving boundaries and interfaces. In: Franca LP, Tezduyar TE, Masud A (eds) Finite element methods: 1970's and beyond. CIMNE, Barcelona, pp 205–220

32. Cruchaga MA, Celentano DJ, Tezduyar TE (2005) Moving-interface computations with the edge-tracked interface locator technique (ETILT). Int J Numer Methods Fluids 47:451–469

33. Tezduyar TE (2006) Interface-tracking and interface-capturing techniques for finite element computation of moving boundaries and interfaces. Comput Methods Appl Mech Eng (published online)

34. Cruchaga MA, Oñate E (1999) A generalized streamline finite element approach for the analysis of incompressible flow problems including moving surfaces. Comput Methods Appl Mech Eng 173:241–255

35. Martin J, Moyce W (1952) An experimental study of the collapse of liquid columns on a rigid horizontal plane. Philos Trans R Soc Lond 244:312–324